JOURNAL OF MATERIALS SCIENCE 29 (1994) 899–920

Effect of fibre misalignment on fracture behaviour of fibre-reinforced composites

Part II *Theoretical modelling*

W. B. HILLIG*
General Electric Company, Corporate Research and Development, Schenectady, New York 12301, USA

When a matrix crack encounters a fibre that is inclined relative to the direction of crack opening, geometry requires that the fibre flex is bridging between the crack faces. Conversely, the degree of flexing is a function of the crack face separation, as well as of (1) the compliance of the supporting matrix, (2) the crossing angle, (3) the bundle size, and (4) the shear coupling of the fibre to the matrix. At some crack face separation the stress level in the fibre bundle will cause it to fail. Other bundles, differing in size and orientation, will fail at other values of the crack separation. Such bridging contributes significantly to the resistance of the composite to crack propagation and to ultimate failure. The stress on the composite needed to produce a given crack face separation is inferred by analysing the forces and displacements involved. The resulting model computes stress versus crack-opening behaviour, ultimate strengths, and works of failure. Although the crack is assumed to be planar and to extend indefinitely, the model should also be applicable to finite cracks.

Glossary of symbols

(Terms used and defined locally may not be listed)

a radius of fibre bundle
C $= 2\tau_f/aE_f$
ε^* critical failure strain of fibre bundle
ε_b bending strain in outer fibre of a bundle
ε_c background strain in composite
ε_f axial strain in fibre
ε_s strain in fibre bundle due to fibre stretching $= \varepsilon_f$
$\varepsilon(\infty)$ strain in composite far from crack
E Young's modulus of fibre bundle
E_c Young's modulus of composite
E_f Young's modulus of fibre
E_m Young's modulus of matrix
$f(\theta)$ number density per unit area of fibres crossing crack plane in interval θ to $\theta + d\theta$
F total force exerted by fibre bundle normal to crack plane
F_s component of fibre stretching force normal to crack plane
F_b component of bending force normal to crack plane
G_m shear modulus of matrix
h crack face opening relative to crack mid-point
h_m matrix contraction contribution to h
h_f fibre deformation contribution to h
h_{max} crack opening at which bridging stress is a maximum
I moment of inertia of fibre bundle
k fibre stress decay constant in non-slip region
k_0 force constant characterizing an elastic foundation (see Equation 7)
L exposed length of bridging fibre bundle (see Equation 1a)
L_f half-length of a discontinuous fibre
m, n parameters characterizing degree of misalignment
N number of bundles intersecting a unit area of crack plane
P_b bending force normal to bundle axis at crack midpoint
P_s stretching force parallel to bundle axis in crack opening
$Q(\phi)$ distribution function describing the degree of misalignment
s_f fibre axial tensile stress
s_f^* fibre tensile failure stress
S stress supported by totality of bridging fibre bundles
S_{max} maximum value of bridging stress
u fibre displacement relative to matrix
u' elongation of fibre in crack bridging region
u_{coh} non-slip contribution to fibre elongation
U fibre elongation due to crack bridging
v overall volume fraction of fibres
v_f volume fraction of bundles

* *Present address:* Rensselaer Polytechnic Institute, Department of Materials Engineering, Troy, NY 12180-3590, USA.

0022–2461

v_m volume fraction matrix between bundles
w transverse deflection of bundle at the crack mid-point
x distance along fibre axis, origin defined by context
X distance between the end of discontinuous fibre and the crack face
X^* threshold (minimum) value of X that results in fibre failure instead of complete fibre pullout
y displacement of fibre normal to its undeflected axis
$Z(\theta)$ area fraction angular weighting function
η tensile strain in fibre relative to applied background strain
η^* critical value of η to cause fibre/matrix debonding
θ angle at which a fibre bundle crosses the crack plane
λ $= (k_0/4EI)^{1/4}$, a parameter in cantilever beam analysis
ν_m Poisson's ratio of matrix
ξ $= \lambda L$ (see Equation 9)
τ shear stress
τ_* interlaminar shear strength of bundle
τ_d fibre/matrix interfacial shear strength
τ_f frictional shear slippage stress at bundle/matrix interface
ϕ angular deviation of fibre bundle from mean orientation of all bundles
ψ angle between symmetry axis and crack plane

1. Introduction

The companion experimental paper [1] pointed out that the idealized configuration of a parallel alignment of reinforcement fibres is not usually achieved in actual unidirectional composites. Monofilament-reinforced composites are an exception in that the interfibre geometry is often controlled by the precise placement of the filament. When multifibre strands are used to make the composite, although the fibres may organize locally into a nearly parallel array, their local orientation generally will deviate from the overall mean direction of the entire fibre population. Each array or bundle in many respects can be viewed as a composite macrofibre. Accordingly, in this paper the terms "fibre" and "fibre bundle" are used interchangeably when, as should be clear from the context, the entire bundle is treated as if it were a single reinforcing fibre.

The stiffness of the neighbouring filaments prevents their "streamlines" from completely filling the space immediately ahead and behind the misaligned bundle. In a non-porous composite this space must therefore be filled by the matrix material. This situation is shown schematically in Fig. 1. Because the matrix material is typically more compliant than is the composite itself, such a matrix-rich pocket tends to accommodate flexure of the fibre as it crosses the gap between the crack faces.

In the case of a polymeric matrices, the elastic moduli are generally orders of magnitude less than those of the reinforcing fibres or fibre bundles. Hence,

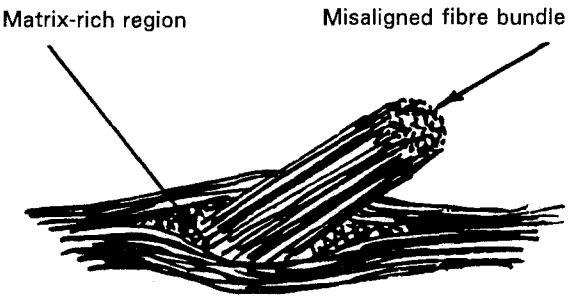

Figure 1 Schematic representation of intersection of a misaligned fibre bundle with its neighbours.

the matrix-rich pockets offer relatively little resistance to fibre bending. When the matrix is a metal, yielding can enhance the compliance. When the matrix is a stiff, non-yielding ceramic or glass, the initial compliance can only be elastic. Direct observation [1] shows that matrix fragmentation can provide the required compliance.

When a matrix crack encounters a fibre that is inclined relative to the direction of crack opening, geometry requires that the fibre flex in bridging between the crack faces. Conversely, the degree of flexing depends on the crack face separation, as well as on (1) the compliance of the supporting matrix, (2) the crossing angle, (3) the bundle size, and (4) the shear coupling of the fibre to the matrix. At some crack face separation the axial stress in the fibre bundle will reach the failure stress level. Other bundles, which differ in size and orientation, will fail at other values of the crack separation. Until a given fibre fails, it is able to carry load and thus contributes to the force resisting the crack opening. The combined contributions of all bundles intersecting the crack determine the resistance of the composite to crack face separation. Thus, fibre bridging contributes significantly to the resistance to crack propagation and to the ultimate strength.

Based on the above concept, the present paper models this resistance, and in particular, considers (1) the effect of misorientation of bundles on filling space, (2) the deformations and load transfer associated with crack bridging by a single misoriented bundle, and (3) the distribution of the fibre orientations. The model is general and, in principle, can treat a wide range of fibre architectures. The present study relates to fibres and matrices that remain fully elastic. The bridging of cracks by obliquely oriented fibres when either the fibres or the matrix are ductile has been considered [2, 3] previously.

The approach taken in the present model is to impose a particular matrix crack face separation, and then to determine from geometrical considerations how the fibre bundle distorts in bridging the gap between the faces. From a detailed consideration of the forces and displacements involved, the stress that must be applied to the composite in order to produce a given crack face separation is inferred. The stress depends on the elastic properties of the bundle and the "matrix", on the coupling between the bundles and the matrix, on the size and orientation of the bundles, and

on other such factors. The resulting model computes stress versus crack-opening behaviour, ultimate strengths, and works of failure. Although the crack is assumed to be planar and to extend indefinitely, the model should be applicable to the consideration of finite cracks as well.

2. Overview of the model

The model assumes that the reinforcing fibres deviate in orientation from their mean direction in a statistically definable way, and that the fibre may be locally grouped into bundles in which neighbouring fibres are parallel. A planar matrix crack is postulated to run either transversely or parallel to the mean fibre direction. The separation of the matrix crack faces increases with increase of the traction applied to the composite normal to the crack plane. As the crack first opens, the fibre response is elastic, reversible, and linear with respect to the crack opening. Symmetry with respect to the reference (unopened) crack plane, allows consideration of only that portion of the composite to one side of the reference plane.

If the bundle is oriented perpendicular to the crack, then pure elongational straining of the bundle will result. However, if the bundle is oriented at an angle to the crack opening displacement, the bundle will experience both an axial and a transverse displacement relative to the position where the axis crosses the crack mid-plane. That is, the bundle must flex in the region between the crack faces. Depending on the crack opening, various irreversible stress-induced processes can occur, such as fibre–matrix debonding, frictional slippage, bundle splitting, or fibre failure. The conditions and sequence of these processes depend on the size and orientation of the bundles, among such other factors as discussed above. At sufficiently large crack openings, the bundles will ultimately fail. The integrated effect of these various responses of the individual bundles will result in a resisting force per unit crack area (i.e. stress) that increases with increasing crack face separation to a maximum value and then decreases with further separation as the fraction of failed bundles increases. The maximum bridging stress, the crack opening distance, and the work of fracture can be calculated from knowledge of the behaviour of the individual bundles and the statistical distributions of their size and orientation.

The plan of the paper is first to analyze the responses of the individual bundles to the opening of the matrix crack. Then a statistical description for quantifying the orientations of the fibre bundles is offered. Assuming that the bundle failures are independent events, the overall response of the composite is integrated into a model. The expectations from the model are compared with experimental data for the failure behaviour of several representative composite systems. However, not all of the required basic input data is available to provide *a priori* estimates of the experimental failure data. In such cases the data is analysed to yield the values of the basic parameters that provide the best fit to the experimental data. The results are then judged for their reasonableness.

Section 3.1 considers the stretching and flexural deformations imposed by geometry as the crack faces separate in detail. The following Section 3.2 estimates the bending force from the amount of flexing that the bundle experiences and also calculates the outer fibre bending strain and the maximum shear stress in the fibre bundle. The bending strain and shear stress can be used to predict tensile failure of the outer fibres or delamination within the bundle. The tensile component of the bundle response is treated in Section 3.3. Fibre–matrix debonding, fibre–matrix frictional slippage and pullout are also considered. The flexural and the tensile resisting forces for a given bundle are combined in Section 3.4 to give the resistance of the bundle to the crack opening.

Because the matrix is stress-free at the crack face, in effect the matrix undergoes an elastic contraction there. This contraction, along with the stretching and bending of the fibre, defines the crack face separation. The contraction is considered in 3.5 and Appendix B.

Statistical representations of the fibre bundle orientations with respect to the crack plane are treated in Section 4. First, distribution functions for the orientational randomness of the fibres are offered. These distributions are then converted into area-weighted distributions for the angles at which the bundles intersect the fracture plane. The results from Sections 3 and 4 are combined in Section 5 to give the overall integrated response. The effects of varying such input parameters as the frictional shear stress and the bond strength are given. Finally, the calculated values for the stress–displacement data are compared with experimental values in Section 5.

3. Crack bridging by a single misaligned bundle

A simple geometric model is used to define the axial and transverse displacements of the bridging fibre. These displacements are introduced into appropriate mechanical models to deduce the stresses, strains, and forces. Depending on the composite, the fibre crossing angle can range from nearly grazing incidence to perpendicular. Simple elastic beam theory can be used at small fibre crossing angles. Under these conditions the lengths of the bridging portions of the fibres are large compared with their diameters or the transverse displacement. At larger crossing angles corrections taking into account the compliance of the matrix in which the fibre is embedded become increasingly important, and corrections to the simple theory follow.

For simplicity and convenience we assume that the individual fibres have an unique characteristic tensile strength value s_f^*.

3.1. Geometric requirements

We consider first the distortion that an inclined bridging fibre experiences as the matrix crack opens. Let the fibre-reinforced composite have an incipient, not yet opened, planar crack, as shown in Fig. 2a. This plane is termed the "crack plane" and remains fixed in space during crack opening. We assume that the crack opens

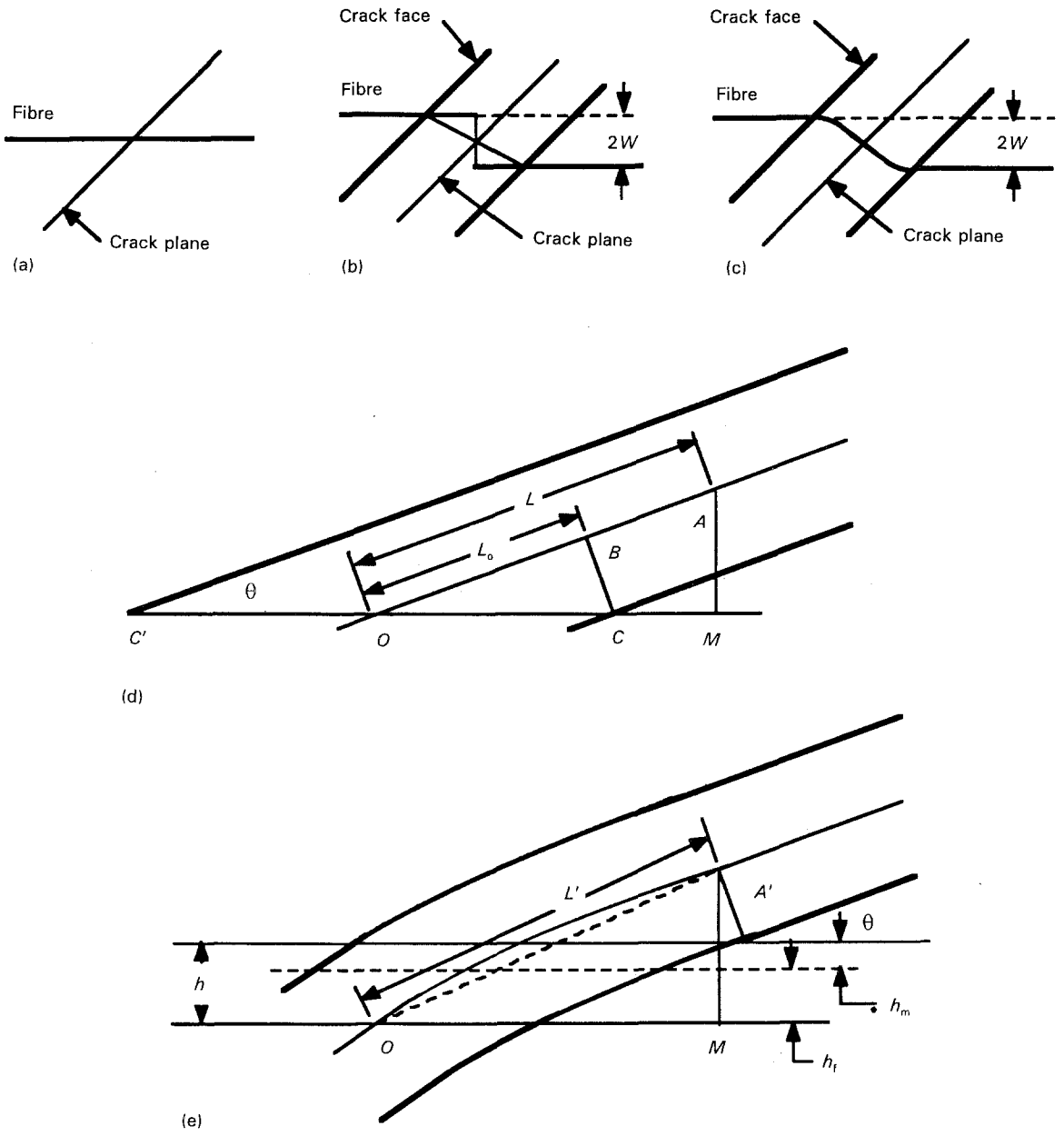

Figure 2 Schematic representation of the geometric distortion experienced by a fibre that is misaligned relative to the direction of the crack opening: (a) the situation prior to crack opening; (b) displacements needed to maintain continuity of the fibre following opening of the crack; (c) the path followed by a continuous fibre in accommodating the crack opening; (d) details of the geometry prior to the crack opening; (e) details of the changes in the geometry in the vicinity of the opened crack.

normal to the crack plane. That is, there is no lateral translation of the crack faces in accord with the assumption that the fibre misorientations are equally probable to either side of the normal to the plane. For the purposes of the present discussion let the matrix that surrounds the fibre be rigid. Thus, the angle at which the fibre enters the crack region remains fixed as the crack opens, i.e. the bundle axes on the opposite sides of the crack remain parallel. However, because the fibre is inclined, the site where the bundle axis enters the crack space translates transversely relative to where the fibre intersected the incipient crack plane prior to crack opening, as is shown schematically in Fig. 2b. The transverse translation is given by $h \cdot \cos\theta$, where θ is the crossing angle relative to the crack plane, and $2h$ is the total crack opening. However, symmetry requires that the intersection of the fibre axis with the crack plane remain fixed in space, as illustrated in Fig. 2c.

How the bundle diameter and the matrix contraction enter into the geometric description are shown in greater detail in Fig. 2d and e. As traction is applied to the composite, the grip ends of the composite translate outwards a distance h_f relative to the situation had cracking not occurred. The distance h_f is the incremental extension of the fibres attributable to the matrix crack. In turn the matrix undergoes a relative contraction of magnitude h_m, because the tensile stress applied directly to the matrix at the crack face is reduced to zero. Thus, the total crack opening is $h = h_f + h_m$.

The fibre bundle must stretch and flex in order to bridge the crack opening. The magnitude of these responses can be deduced from geometric consider-

ations. The fibre geometry prior to crack opening is shown in Fig. 2d. The fibre axis intersects the incipient crack plane at O; the outer diameters intersect the plane at C and C', which are the sites at which the fibre emerges from the support provided by the rigid matrix. We define the point O to be the origin of a Cartesian coordinate system. Let the x axis lie in the crack plane and the y axis be normal to the plane. In order to accommodate flexure of the bundle, we postulate limited fibre–matrix debonding above the crack plane in the vicinity of C' and below the plane at C. As the crack opens, the bundle flexes similarly about the support points C and C' leading to a bundle shape that has a center of symmetry at O. (The restriction that the bundle is rigidly supported until it enters the crack opening region will be removed later. This also relaxes the postulate regarding fibre–matrix debonding.)

In considering the flexure of the bundle, we focus on the trajectory of the bundle axis, noting that the fibre is supported by the matrix up to points C and C' and taking into account the effect of the fibre radius a. Thus, when the crack begins to open, the onset of flexure occurs at point B on the fibre axis. The coordinates of B are designated $[x(B), y(B)]$ and have the values $a\cdot\cos\theta/\tan\theta$ and $a\cdot\cos\theta$, respectively. The length of the segment OB is L_0 and equals $x(B)/\cos\theta = a/\tan\theta$.

Now let the crack open the finite distance h, as a result of a matrix displacement h_m and a fibre displacement h_f, as shown in Fig. 2e. The matrix displacement causes the onset of flexure to shift laterally a distance $h_m/\tan\theta$ to the position M at the crack face, or to position A along the fibre axis. Thus, $x(A) = x(B) + h_m/\tan\theta$, where $x(A)$ is the x coordinate of both points A and M.

Prior to crack opening the length L of the segment OA was $x(A)/\cos\theta$, given by

$$L = a/\tan\theta + h_m/\sin\theta \qquad (1a)$$

and the y coordinate of $A = y(A) = x(A)\tan\theta$. The quantity L is the length of fibre segment that will bridge the crack, measured prior to the actual bridging. Thus, L serves as the reference length in considering the flexural and tensile responses of the fibre. After the crack opening the point A does not move laterally. However, relative to the crack plane it moves normally a distance h_f. The point A after crack opening is denoted A' and has the coordinates $[x(A'), y(A')]$, where $x(A') = x(A)$ and $y(A') = y(A) + h_f$. The segment length OA' equals L', and is

$$L' = \sqrt{(x(A')^2 + y(A')^2)}. \qquad (1b)$$

3.2. Flexural deformation

At shallow crossing angles $L/a \gg 1$, allowing the bundle to be modelled as a simple end-loaded cantilever beam. However, as the angle increases, L/a decreases; the elementary beam equations become increasingly inaccurate in relating the bending force to the transverse displacement. The simple model is given first, followed by an analysis that includes flexing of the bundle within the (compliant) supporting wall.

3.2.1. Fibre crossing at small angles

In this section, for the purposes of considering the fibre bundle as a beam, we define a new Cartesian coordinate system lying in the place of the flexure, in which origin coincides with the point of fibre crossing with the crack plane, the x-axis is parallel to the fibre axis far from the crack zone, and y is the transverse displacement as a function of distance x from the origin. As the crack faces move apart, geometric continuity and symmetry require (1) that the trajectory of the fibre $y(x)$ be an odd function, (2) that the slope y' be a maximum at $x = 0$, and (3) that the slope at A', where the flexed fibre joins that of the embedded fibre, matches that of the embedded misaligned fibre. (As discussed above, we assume at least local debonding in the vicinity of C between the fibres and the matrix.) These conditions are satisfied by

$$y = jx - kx^3 \qquad (2)$$

Such a displacement law is identical to that of two opposing cantilever beams that are built into the composite (assumed rigid) at C in the upper crack face and at the symmetrical site on the lower face of the crack. Each cantilever terminates at the origin, where each loads the other by the amount required by the crack opening, as depicted in Fig. 2b.

Using the cantilever equivalence allows the bending force at $x = 0$ to be estimated from the familiar beam equations when the beam (bundle) length is large compared with its radius. From Equation 1 it is seen that $L/a > \cot\theta$. Thus, for example, at $\theta = 3°$, $L/a > 20$. The normal force P_b applied at $x = 0$ is given in terms of the deflection w of the end of the beam through

$$P_b = 3wEI/L^3 \qquad (3)$$

where I is the moment of inertia and E is the Young's modulus of the bundle parallel to its axis. Inspection of the geometry given in Fig. 2b shows that $w = h\cos\theta$. The component of P_b normal to the crack is the bending force component that resists opening of the crack.

The local outer fibre strain ε_b due to bending is given by the product of the bundle radius and the local curvature due to bending, i.e. $\varepsilon_b = ay''$. The maximum flexure occurs at A', where the outer fibre tensile strain is

$$\varepsilon_{b,\max} = 3ah_f\sin^2\theta\cos\theta/(a\cos\theta + h_m)^2 \qquad (4)$$

3.2.2. Compliant matrix support of fibre bundle

The preceding analysis ignores the effect of the compliance of the material that surrounds the fibre bundle. As already discussed, without some compliance and/or debonding, no crack opening is possible without rupturing or plastically deforming the bundle. The problem of a cantilever beam made of one material that is built into an elastic "wall" made of a second

material appears not to have been solved. However, the related problem of a beam resting on an elastic foundation has been extensively examined [4], including the case where both the beam and the foundation extend from a given point to infinity. In this context the term "elastic foundation" means a support such that a transverse displacement of the beam results in a reaction force that is proportional to the displacement. The force constant for the foundation can be estimated [5] from its elastic properties. This analysis can be utilized by extending the beam a finite distance into the free space beyond the foundation, and imposing a transverse deflection w at the free end. The transverse force P_b required to produce that deflection and the maximum bending strain in the bundle can then be calculated.

Let the longitudinal and transverse coordinates of the axis of the bundle supported by the foundation be given by (x_1, y_1), the corresponding coordinates for the free portion of the bundle by (x_0, y_0), and the boundary between the two regions by $x_1 = x_0 = 0$, i.e. x_0 and x_1 represent absolute distances from the boundary. Geometric continuity requires $y_0(0) = y_1(0)$, and $dy_0/dx_0 = -dy_1/dx_1$ at $x_0 = 0$. The application of the force P_b at the free end, where $x_0 = L$, imposes a bending moment P_bL, and a shear force P_b in the beam at the boundary, i.e.

$$y_1''(0) = P_bL/EI \quad (5a)$$

and

$$y_1'''(0) = P_b/EI \quad (5b)$$

where the primes indicate differentiation with respect to x.

The general solutions for $y_0(x_0)$ and $y_1(x_1)$ are

$$y_0 = P(L - x_0)^3/6EI + b_1x_0 + b_2 \quad (6a)$$

and

$$y_1 = \exp(-\lambda x_1)[c_1\cos\lambda x_1 + c_2\sin\lambda x_1] \quad (6b)$$

where b_1, b_2, c_1, c_2 are constants to be determined. The quantity $\lambda = (k_0/4EI)^{1/4}$; k_0 is approximately given in terms of the shear modulus of the matrix G_m by

$$k_0 = (\pi/2)^2G_m/0.95(1 - \nu_m) \quad (7)$$

Introducing these conditions into the above relationships leads to

$$y_0(x) = \beta\{Lx^2/2 - x^3/6 + [(1 + 2\xi)/2\lambda^2]x + (1 + \xi)/2\lambda^3\} \quad (8a)$$

$$y_1(x) = (\beta/\lambda^3)\exp(-\lambda x)[\cos\lambda x + \xi(\cos\lambda x - \sin\lambda x)] \quad (8b)$$

where the subscripts to x have been dropped, $\beta = P/EI$, and $\xi = \lambda L$. Noting that $y_0(L) = w$, the displacement at the boundary and the transverse force are given by

$$y_1(0) = \beta(1 + \xi)/\lambda^3 \quad (9)$$

and

$$P_b/w = 3k_0L/[4\xi^4 + 6\xi^2(1 + 2\xi) + 6\xi(1 + \varsigma)] \quad (10)$$

When θ approaches $\pi/2$, L and hence ς both approach 0. It follows from Equation 10 that the ratio P/w remains finite. However, because $w = h\cos\theta$, it also follows that w and P vanish together. Thus, as θ approaches either 0 or $\pi/2$, the bending force vanishes.

The maximum curvature and bending strain occurs at the boundary, and using the Bernoulli–Euler relationship, this strain ε_b is readily calculated from Equation 10 through

$$\varepsilon_b = ay''(0) = P_baL/EI \quad (11a)$$

Recalling the expressions for λ and w, and making use of Equation 1a, at the limit of large L the expression for ε_b is seen to reduce to Equation 3. However, at small L ε_b tends to

$$\varepsilon_b = ah_f(a\cos\theta + h_m)/[(1 + \xi)\lambda^3\tan\theta] \quad (11b)$$

and becomes zero at the limit $\theta = \pi/2$. Differentiating with respect to ξ, shows that ε_b is a maximum when $\xi = 0.5979$, and

$$\varepsilon_{b,max} = 0.0326(3k_0aw/EI\lambda^2) \quad (11c)$$

The dependence of ε_b on θ is given in Fig. 3 for the case of a representative composite reinforced with 50 volume per cent fibre bundles in which the fibre content is 80 volume per cent. The plot shows that the maximum bending (tensile) strain depends approximately logarithmically on the E/G stiffness ratio. When this ratio equals 0.1, and the crack opening equals the bundle radius, the maximum strain exceeds 0.1 and occurs at a crossing angle of about 26°.

3.2.3. Bundle integrity

During flexure fibre bundles may break up into subbundles or individual fibres as a result of shear debonding failure. We postulate the existence of a threshold shear stress τ^* for initiating such intrabundle delamination. Beam theory gives the shear stress on the beam axis to be a maximum, which is

$$\tau = P_ba^2/2I \quad (12)$$

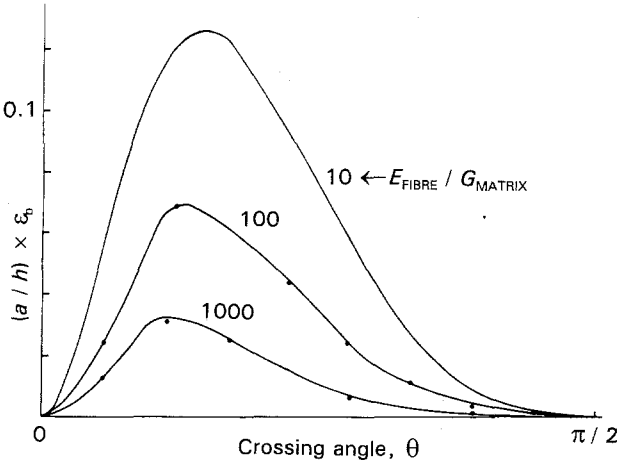

Figure 3 Dependence of the bending strain E_b on the bundle crossing angle θ.

From Equations 10 and 12 the condition for bundle delamination in terms of crack opening and θ can be determined. If delamination occurs, each half in effect becomes a new bundle, requiring that I be redetermined. Other shearing or buckling mode failures are possible, but are not considered in the present model.

3.3. Tensile deformation

The crack opening h is treated as an independent parameter and is the sum of the fibre extension h_f and the matrix contraction h_m relative to the geometry prior to matrix cracking. If the entire fibre remains coherent with the matrix, the fibre displacement is purely elastic and reversible. However, once the fibre is debonded from the matrix, the debonded portions of the fibre can slide relative to the matrix. The resistance to such sliding can be characterized by a frictional shear stress τ_f, assumed for simplicity to have a fixed value. Recall that the fibres may be oriented at any angle θ relative to the crack plane, and that the applied stress is normal to the crack plane. The problem is to determine the fibre axial stress in the crack bridge region using known values of h, τ_f, and other physical and elastic properties.

As the crack faces open, the fibre bundles must bend as well as elongate. The elongation can be determined from the increase in the line integral along the fibre axis trajectory as the crack opens. Compliance of the surrounding matrix material partially relaxes the severity of the bending required as the fibre bundle bridges the gap between the crack faces. In principle, the amount of stretching is also reduced. However, line integration over the bent region, using the lateral displacements given by Equations 8a and 8b, shows that reduction of the axial elongation is negligible.

Hence, the elongation can be adequately and more simply approximated by means of the constructions shown in Fig. 2d and e, which schematically compare the bundle geometry before and after the crack has opened an amount $h = h_f + h_m$. Equations 1a and 1b, respectively, give the length L of a given segment of the bundle prior to crack face separation, with the length L' of the fibre in the unstressed state, and Equation 1b gives the length L' of the same segment after crack opening. Thus, the fibre elongation U is $L' - L$, allowing U to be calculated with an error of less than 20% relative to results from line integration by

$$U \approx h_f \sin\theta \tag{13}$$

provided that $(h_f/a) < 1/2$.

This geometrically prescribed elongation must be accommodated by the amount of incremental stretching u' of the fibre in the crack-bridging region caused by the straining of the fibre, and by u, the differential displacement of the fibre relative to the matrix within the composite. That is, $U = u' + u$. The term u' is relatively more important during the initial stages of crack opening, but can be neglected with little error once substantial fibre–matrix slippage occurs.

It is given by

$$u' = L\eta(0) \tag{14}$$

where $\eta(x)$ including $\eta(0)$ is defined by

$$\eta(x) = \varepsilon_f(x) - \varepsilon_f(\infty) \tag{15}$$

in which x is the axial distance along the fibre measured from the crack face, $\varepsilon_f(x)$ is the fibre strain at x, and $\varepsilon_f(\infty)$ is the fibre strain far from the influence of the crack. The term u depends on how the fibre is coupled to the matrix.

As is discussed more fully in Appendix A, the inability of the matrix to carry stress across the crack faces requires that the bridging fibres carry an increased tensile load in that region. This excess fibre stress is ultimately transferred back to the matrix within the composite at a rate that depends on the fibre–matrix coupling. An excess fibre strain, given by $\eta(x)$, parallels the excess stress, and causes the fibre to elongate relative to the case when the composite remains uncracked. It is this differential elongation that allows the fibre to bridge the gap between the crack faces. The interrelations between the coupling, the crack opening, and the fibre stress $s_f(x = 0)$ are developed next.

3.3.1 Fibre bundle well-bonded to the matrix

When the fibre is coherently bonded to the matrix, the fibre strain decays exponentially with distance from the crack face. The decay constant k is discussed in Appendix A, and is a function of the fibre volume fraction, of the elastic properties of the fibre bundle and the matrix, and of the bundle radius. In the absence of fibre–matrix slippage to the matrix, when the fibre is coherently coupled, the fibre extension u_{coh} is (see Equation A10b)

$$u_{coh} = \eta(0)/k \tag{16}$$

and the shear stress acting on the fibre at $x = 0$ is

$$\tau(0) = E\eta(0)ak/2 \tag{17}$$

For an inclined fibre $\varepsilon_f(\infty)$ is the strain ε_c in the composite, far from the crack, resolved parallel to the fibre axis, i.e.

$$\varepsilon_f(\infty) = \varepsilon_c \sin^2\theta \tag{18}$$

where $\varepsilon_c = S/E_c$, S is the stress applied to the composite normal to the crack plane, and E_c is the corresponding Young's modulus of the composite.

In the present case $u = u_{coh}$. We evaluate $U = u' + u$ by introducing the expressions for the separate terms to yield

$$\eta(0) = h_f \sin\theta/(L + 1/k). \tag{19}$$

The stress $s_f(0) = E\varepsilon_f(0)$ carried by the fibre bridge can now be determined in terms of h_f and ε_c.

When the calculated value of $\eta(0)$ is such that $\tau(0) > \tau_d$, then fibre debonding and frictional sliding can occur, τ_d being the critical shear stress for fibre–matrix debonding. This critical shear stress has been shown [6] to be uniquely related to the surface work of debonding. It follows from Equation 17 that debonding can commence when $\eta(0)$ in turns reaches a critical value η^* given by

$$\eta^* = 2\tau_d/akE \tag{20}$$

Once substantial fibre–matrix slippage occurs, u_{coh} makes a minor contribution to U.

3.3.2. Frictional coupling between fibre bundle and matrix

The frictional coupling between the fibre and its surroundings is characterized by a resisting frictional shear stress τ_f, which we assume to be constant. The strain in the fibre as a function of distance x from the crack face is

$$\varepsilon_f(x) = \varepsilon_f(0) - Cx \quad (21a)$$

in which C is an abbreviation C defined by

$$C = 2\tau_f/aE_f \quad (21b)$$

The corresponding stress $s_f(x)$ is $E_f\varepsilon_f(x)$. The fibre displacement u at the crack face when debonding can occur is given by Equation A15, namely

$$u = (\eta^2(0) - \eta^{*2})/2C + u_{coh} \quad (21c)$$

We again set $U = u' + u$ and use Equations 13, 14, and 16 to yield the quadratic expression

$$\eta^2(0) + A_1\eta(0) - B_1 = 0 \quad (22)$$

where $B_1 = 2Ch_f \sin\theta + \eta^{*2} - 2C\eta^*/k$ and $A_1 = 2CL$. An expression for the exponential elastic strain decay constant k has been given by Budianski *et al.* [7] (see Appendix A, Equations A6a–c) in terms of the fibre radius, fibre volume fraction, and the elastic constants of the constituents. An alternative formulation is offered in Appendix A, Equations A9a–c.

For convenience in presenting the solution to Equation 22, we express the various input factors in terms of the following dimensionless parameters: $\alpha = \tau_f/\tau_d$; $\beta = h_m/h_f$; $\gamma = \tau_d/E_f$; $r = h_f/a$. Some quantities are experimentally known; in principle all are measurable.

The solution for $\eta(0)$ when $r < 2\gamma/k^2 \sin\theta$ is given by setting $L = 0$ in Equation 19. For larger values of r

$$\eta_0 = [\psi_0^2 + \psi_1 + \psi_2]^{1/2} - \psi_0 \quad (23)$$

$$\psi_1 = (\gamma/k)^2(1 - 2\alpha)$$

and $$\psi_2 = 4\alpha\gamma\omega\sin\theta.$$

When $\eta(0) \gg \eta^*$, it follows from Equation 21c that

$$\eta(0) = [\alpha\gamma\omega\sin\tau + (\gamma/ak)^2]^{1/2} \quad (24)$$

In these expressions $\eta(0)$ increases monotonically from zero when $\theta = 0$ to a limiting value as θ increases to $\pi/2$. Fig. 4a and b shows the dependence of $\eta(0)$ on θ using input G_m/E_f ratios of 0.003 and 0.1 as being representative of polymeric and ceramic matrix composites, respectively. For both examples we set v_f equal to 0.5, and α to 0.1 or less (sliding friction cannot exceed the initial debond shear stress). The debond shear stress τ_d is estimated to range from 0.001 to 0.1 of the matrix shear modulus for both polymeric and ceramic systems, and β to be in the approximate ratio of E_f/E_m, namely 30 and 1 for the polymeric and ceramic systems, respectively. The value selected for r is 0.1, which from Equations 17 and 19 leads to values of $\tau(0)$ that far exceed the τ_d values predicted to initiate debonding in either system when $\theta = \pi/2$. Fibres oriented normal to the crack debond prior to those inclined to the crack.

Fig. 4a and b shows that decreasing either τ_d or τ_f, while holding the other shear constant fixed, results in a decrease of $\eta(0)$ for all values of θ. However, the shape of the curve can vary considerably depending on other parameters. The effect of increasing v is to increase k and in turn to decrease $\eta(0)$, as shown in Fig. 5. The magnitude of the effect varies with the values of τ_d and τ_f. Although trends can be qualitatively discerned, caution is required, because the

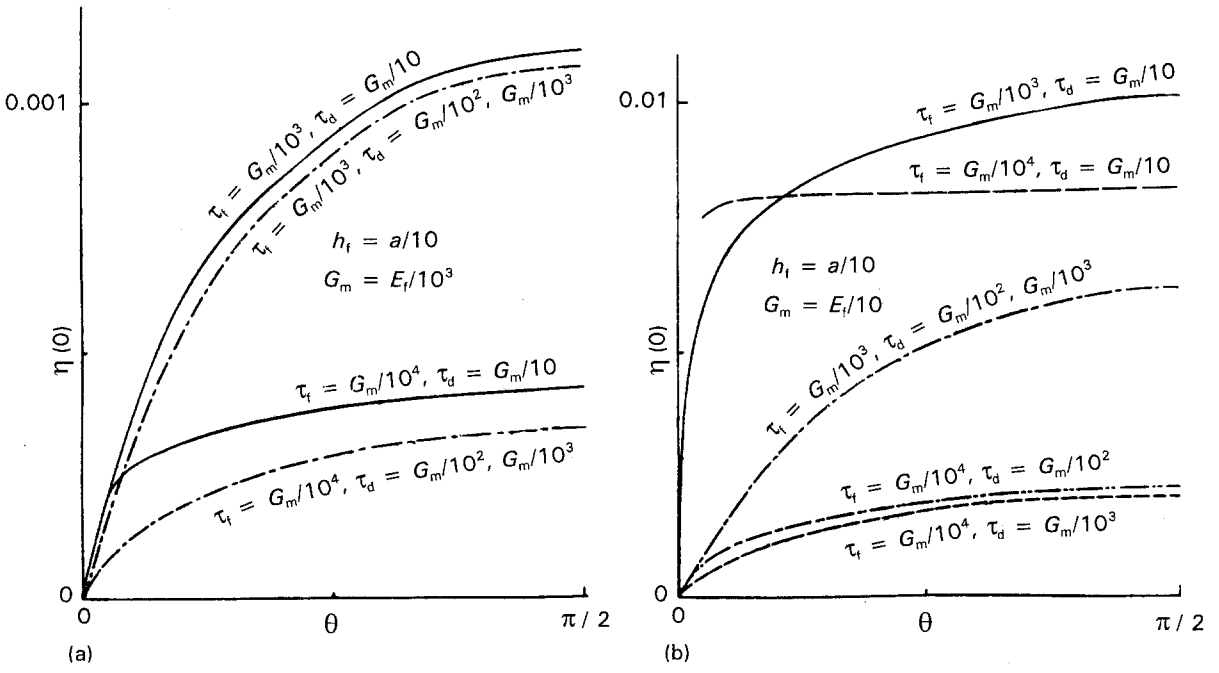

Figure 4 The effect of the fibre debond shear stress τ_d and the frictional shear stress τ_f on the bundle excess tensile strain $\eta(0)$ in the crack bridging region relative to the bundle strain far from the crack as a function of fibre crossing angle θ when (a) the matrix is much more compliant than the fibre, and (b) the matrix is comparable in stiffness to the fibre.

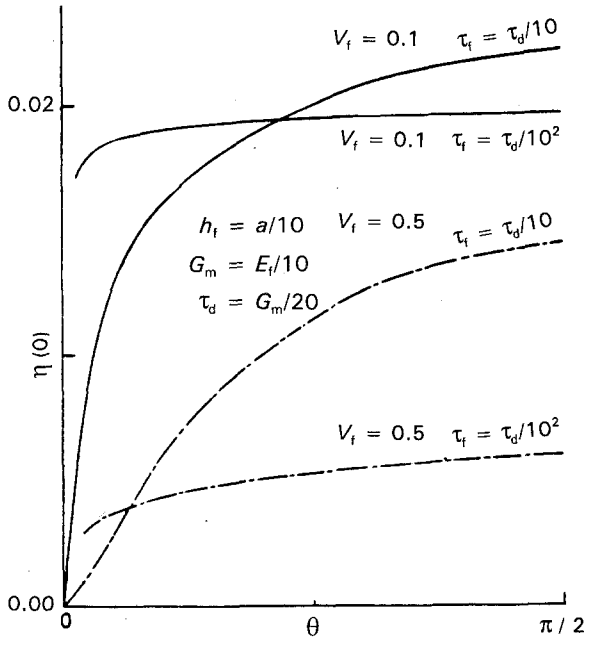

Figure 5 The effect of fibre volume fraction v_f and the frictional shear stress τ_f on the bundle excess tensile strain $\eta(0)$ in the crack bridging region relative to the bundle strain far from the crack as a function of fibre crossing angle θ for fibre when the matrix is comparable in stiffness to the fibre.

relative importance of the various parameters is complicated by the overall composite characteristics and the applied stress.

3.3.3. Discontinuous fibre bundles frictionally coupled to matrix

The above model can be extended to include discontinuous reinforcing fibres. The case of discontinuous unidirectional fibres oriented parallel to the direction of the applied tensile stress has been treated by Cooper [8]. The discussion that follows extends that treatment to randomly oriented fibres. A more detailed analysis is given in Appendix A3.

We consider that (1) the discontinuous fibres have the same length $2L_f$, and (2) that the ends of the fibres are located at random distances from the crack plane. (All lengths and distances here and below are measured along the fibre.) Thus, that end of a fibre that is closest to the crack lies at a distance $L_{f,i}$ from the crack plane, where $0 < L_{f,i} < L_f$. The tensile stress in the crack-opening region depends on the fibre orientation, on the distance L that the fibre is exposed in that region, and on distance X_i over which the fibre is embedded in the matrix. Thus, X_i is simply $L_{f,i} - L$, as is evident from Fig. 6. Finally, the distance along which the fibre is only frictionally coupled to the matrix is L_s, where $L_s \leq L$.

In bridging the gap between the crack faces, the discontinuous fibres (bundles) stretch in response to the applied stress. They can also slide out of their "sockets", providing that their embedded length X_i is less than a critical value X^*. The quantity X^* is such that stress in the crack-opening region just fails to cause fibre failure. This condition is satisfied when

$$X^* \leq s_f^* a/2\tau_f - [\varepsilon(\infty) - \eta^*]/C \qquad (25)$$

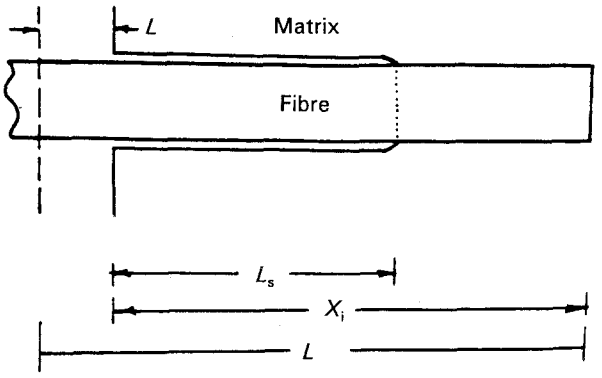

Figure 6 Schematic diagram of a partially debonded, discontinuous, crack-bridging fibre that defines the various parameters.

from Equations 20 and 21; s_f^* is the fibre failure stress.

Should X_i lie farther than X^* from the crack face, then the situation will be essentially the same as if the fibre were continuous. Equation 24 can then be used to calculate $\eta(0)$, and in turn $s_f(0)$. For values of X_i less than X^*, the pullout stress s_{po} is given by

$$s_{po} = E_f[\varepsilon(\infty) + \eta^*] + CE_f X_i \qquad (26)$$

The analysis of the bending strains is the same for continuous fibres (see 3.2). Obviously, once fibres have been totally pulled out, their stretching and bending contributions to the bridging stress vanish.

3.3.3.1. Fibre failure precluded. Fibre failure is precluded if X_i is so small that the fibre stress at the crack is less than the fibre tensile strength s_f^*, i.e. if $X_i < X^*$, and $X^* = s_f^* a/2\tau_f$. For fibres meeting this criterion, as the crack opens the fibres become increasingly exposed over a distance L in the crack opening region, as shown in Fig. 5. Any fibres for which $L_{f,i} < L$ would be completely extracted. The fibre stress $s_f(0)$ at the crack face is given by $2\tau_f X_i/a$, as long as X_i remains less than the critical value X^*. For larger values of X_i fibre failure will occur in the crack bridging region.

For a random distribution of fibre end positions, the mean fibre stress at the crack face is

$$\langle s_f(0)\rangle = [1 - as_f(0,X)/4\tau_f L_f - L/L_f]s_f(0,X) \qquad (27)$$

where $s_f(0,X)$ is the fibre tensile stress at $x = 0$, when the maximum distance between the ends of bridging fibres and the crack plane is X.

As the crack opens, L increases, and X_i decreases. The point is finally reached where, for those fibres for which $X_i < X^*$, further crack opening causes a decrease of $s_f(0)$. In this regime the mean fibre stress is given by

$$\langle s_f(0)\rangle = \tau_f(L_f - L)^2/aL_f \qquad (28)$$

Thus, as the crack opens the resisting force goes through a maximum and vanishes when all of the fibres have been pulled out.

3.3.3.2. Fibre failure possible in addition to pullout. If the fibres are longer than $2X^*$, some will be situated

such that even the closest end is farther than X^* from the crack face. Those fibres will fail in tension prior to pullout. For crack openings insufficient to develop stress levels that will cause fibre failure, the situation is the same as that discussed for the previous case. However, when the calculated $s_f(0)$ exceeds the fibre strength s_f^*, then

$$\langle s_f(0)\rangle = (L^* + s_f^* a/2\tau_f - L)^2 \tau_f/a \quad (29)$$

where L^* is the value of L when $s_f(0) = s_f^*$. In all cases the effective mean strain $\langle \varepsilon_f \rangle$ is simply $\langle s_f(0)\rangle/E_f$.

3.4. Load transfer across crack

Fibre bundle failure is postulated to occur where the total strain caused by stretching plus flexing is greatest. The bending force has been given by Equation 10. The corresponding stretching force is related to ε_f or $\langle \varepsilon_f \rangle$ (see Equations 20–24) by

$$P_s = \pi a^2 E \varepsilon_f \quad (30)$$

The total force F that the bundle supports in bridging the crack is the sum of the bending and stretching forces normal to the crack plane and is simply

$$F = P_b \cos\theta + P_s \sin\theta = F_b + F_s \quad (31)$$

which defines the normal forces F_b and F_s, and where P_b and P_s are given by Equation 30 and Equations 31, 6, or 12. If the failure strain ε^* of the fibre bundles is a fixed material property, then

$$\varepsilon_b + \varepsilon_s = \varepsilon^* \quad (32)$$

defines the condition for the failure of a single fibre, or for failure of the outer fibre of a fibre bundle. These latter two equations provide the basis for calculating the maximum crack opening and the ultimate force that a bundle can carry.

A more realistic treatment, beyond the scope of the present paper, would consider the effect of flaw distribution on the failure strain and failure sites.

3.5. Estimation of matrix displacement relative to fibre extension

Both displacements h_f and h_m enter into the expressions for the fibre bending and axial strains. In order to compute those strains from a knowledge of h_f, it is necessary to relate h_m to h_f. Thus far, h_f and h_m have been treated as independent variables. In the case of an ideal unidirectional composite having the reinforcement oriented normal to the crack, h_m can be related to h_f through the requirement for static equilibrium (see Appendix B, Equation B7) by

$$h_m = (v_f E_f)/(v_m E_m) h_f \quad (33)$$

This ideal unidirectional model assumes that the fibre and matrix displacement are normal to the plane of the initial matrix crack and as the crack opens, the faces remain planar and parallel. However, when the individual bundles are not normal to the crack plane, the situation is more complicated.

Appendix B offers the following expression as an estimate of the dependence of h_m on h_f when the fibres cross the fracture plane over a statistically defined range of values

$$\langle h_m/h_f \rangle_{Ave} = \frac{\int_0^{\pi/2} \left[\frac{E_c(\theta)}{V_m E_m} - 1\right] Z(\theta) \sin^2\theta \, d\theta}{\int_0^{\pi/2} Z(\theta) d(\theta)} \quad (34)$$

in which $E_c(\theta)$ is the dependence of the Young's modulus of a unidirectional composite on the angle θ between the fibres and the applied tensile stress. The term $Z(\theta)$ is the weighting function for the area fraction of bundles crossing a unit area of crack surface at the angle θ, as given by Equation 37. Inasmuch as h_f is an independent variable, the above equation allows h_m and h to be determined. The composite modulus $E_c(\theta)$ can be estimated [9] from the properties of the matrix and the reinforcement.

4. Distribution of fibre bundle orientations

One way to characterize a given fibre bundle is to specify its radius a and its misorientation angle ϕ relative to a vector representing the mean direction of all bundles. The vector is assumed to be an axis of rotational symmetry for the bundle deviations from perfect alignment. The distribution of the values of a and ϕ can be used to characterize the composite. However, it is the distribution of θ (i.e. the angle that the bundles make in crossing the crack plane) that is of present major interest. For convenience, although not necessary, we treat the bundles as if they all had the same cross-sectional area given by the average value.

For determining parametric dependencies it is convenient to begin by specifying the misalignment probability $Q(\phi)$ to calculate the number density of fibres crossing the crack plane in an angular interval $d\theta$ centered around θ. However, knowledge of $Q(\phi)$ is not absolutely essential, because this number density $f(\theta)$ is experimentally measurable. Nevertheless, insight is gained by relating the crossing angles θ back to the underlying misalignment ϕ angles. The applied stress on the composite, which is balanced by the force per unit area supported by the bridging fibres, is determined by integrating $f(\theta)$ times (the force carried per bundle normal to the crack) with respect to θ. A more complete discussion is found in Appendix C.

4.1. Fibre misalignment functions

Let us consider the spatial orientations of the fibre bundles in terms of a stereographic representation. Let ϕ be the angular deviation of a given fibre bundle from the unit vector corresponding to the mean bundle direction. The vector has its origin at the center of a sphere of unit radius. Where the vector intersects the surface of the sphere defines the reference point. Similarly, a misaligned fibre is represented by a similar vector, but oriented at an angle ϕ. Its intersection with the surface produces another point on the sphere. Other fibres will generate other points. We assume that the pattern of points is symmetrical around the reference point, that the density of points per unit surface area is a continuous function $Q(\phi)$ of angular

distance from the reference point, and that the cross-sectional area of matrix associated with a fibre is independent of its orientation.

If $Q(\phi)$ has a maximum corresponding to the mean fibre direction (i.e. $\phi = 0$), then the distribution is prolate or quasi-unidirectional. If Q has a maximum at $\phi = \pi/2$, then the distribution is oblate or quasi-2-dimensionally random. If Q = constant for all ϕ values, then the distribution is 3-dimensionally random. Many other distributions are possible.

We next define ψ as the angle which the unit vector representing the axis of fibre symmetry makes with respect to the crack plane and θ as the angle that a particular fibre makes relative to the crack plane. The angle ψ in combination with $Q(\phi)$ fixes $f(\theta)$. When $\psi = 0$, the axis of symmetry lies in the crack plane; for a prolate distribution this corresponds to a splitting mode of fracture, but for an oblate distribution this corresponds to transverse fracture. When $\psi = \pi/2$, the fracture modes are the reverse, namely the prolate distribution experiences transverse fracture, and the oblate distribution fails by splitting. For $\psi = 0$ or $\pi/2$ the transformation between the $Q(\phi)$ and the $f(\theta)$ function is relatively simple. Experimentally, these ψ values are the most likely values to be encountered. Arbitrary values of ψ complicate the translation from Q to f and are not included here. However, the results could be of interest for examining the stability of the splitting and transverse modes.

When the symmetry axis is perpendicular to the crack plane, i.e. when $\psi = \pi/2$, the misalignment angle ϕ equals $(\pi/2 - \theta)$. For this case it can be readily shown that

$$f(\theta) = kQ(\pi/2 - \theta)\cos\theta \tag{35}$$

When $\psi = 0$, then $f(\theta)$ is given by

$$f(\theta) = \cos\theta \int_{\pi/2-\theta}^{\pi/2} \frac{Q(\phi)\sin\phi\,d\phi}{\sqrt{\cos^2\theta - \cos^2\phi}} \tag{36}$$

where in either case if Q is expressed purely as a trigonometric factor, the constant K is needed to relate $f(\theta)$ to the density of fibres. Correspondingly, the areal distribution function $Z(\theta)$ is given by

$$Z(\theta) = \pi a^2 f(\theta)/\sin\theta \tag{37}$$

If N is the total number of fibres crossing a unit area of the crack plane, then

$$\int_0^{\pi/2} f(\theta)d\theta = N \tag{38}$$

Inasmuch as

$$\int_0^{\pi/2} Z(\theta)d\theta = v \tag{39}$$

where v is the area fraction occupied by fibres per unit area of crack plane. Thus, the number of fibres per unit area crossing at $\theta \mp d\theta/2$ is given by $F(\theta)$ as

$$F(\theta) = vf(\theta) \Big/ \int_0^{\pi/2} Z(\theta)d\theta \tag{40}$$

4.2 Relations between specific axial and planar crossing distributions

We now discuss various types of representations of $Q(\phi)$, as shown schematically in Fig. 7, and their relation to $f(\theta)$. If a prolate distribution extends over a wide range of angles, the form $Q(\phi) = \cos^m\phi$ is convenient for performing the above integrations. The

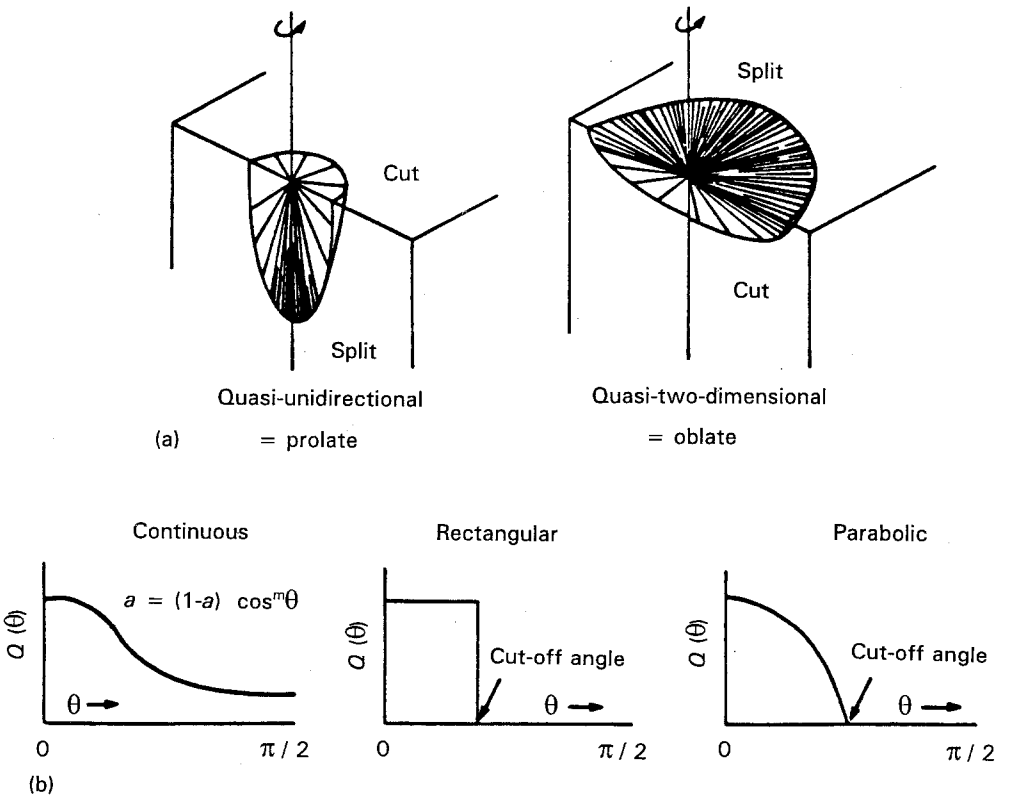

Figure 7 Diagrammatic representation of the various fibre orientation functions.

effective range of the distribution can be narrowed by increasing m. The angle $\phi_{0.5}$, where the magnitude of $Q(\phi)$ is half its maximum value, is given by $\phi_{0.5} \sim (\pi/3)/\sqrt{m}$. To reduce $\phi_{0.5}$ to $\pi/6$ requires $m \sim 5$, and to reduce it to $\pi/12$ requires $m \sim 20$.

Similarly, $Q(\phi) = (1 - \cos\phi)^m$ can be conveniently used to describe a broad oblate distribution. In this case $\phi_{0.5} \sim (\pi/2) - \pi/6m$, which shows that this distribution narrows more rapidly as m increases relative to the above distribution. Alternatively, spherical harmonics can be used [10].

For the above cases the $Q(\phi)$ and the corresponding $f(\theta)$ distributions are given in Tables I and II. Constant multiplying factors have been omitted.

5. Total response of composite

As the crack first opens, the separation is accommodated by purely reversible elastic deformation. Further separation causes frictional slippage of the fibre bundle relative to the matrix, bundle splitting, or bundle failure. Continuous bundles oriented approximately normal to the crack can support a load in that direction that approaches their breaking strength. Pullout may intervene if the bundles are discontinuous, or if the bundle failure is assumed to occur at random flaws. At the other extreme, bundles oriented nearly parallel to the fracture plane can remain bridging over large crack openings, but the force they exert normal to the crack plane is accordingly less.

Progressive failure of the constituent bundles proceeds via various essentially independent processes, each of which depends on a multiplicity of physical properties. Hence, it is not feasible to combine these elements into an analytic model. Nevertheless, the various factors discussed above can be integrated into a computer model, taking as inputs: (a) fibre, matrix, and composite elastic properties; (b) diameter, aspect ratio, and volume fraction of the fibre bundles; (c) the degree of misorientation of the bundles; (d) the bond shear strength and the frictional shear coupling between the bundles (or fibres) and the matrix; (e) the interlaminar shear strength of the fibre bundles. The output of interest is the mean force exerted by the bridging fibres and the external work expended as a function of crack-face separation. The overall model can be used for parametric studies, guidance of materials development, or estimates of composite behaviour, or conversely, to estimate the values of the underlying controlling parameters from experimental data for the composite.

Calculated results of the relationship between the bridging stress and the crack-opening displacement are shown below in Section 5.1 using input parameter values appropriate for some representative composites. The following Section 5.2 presents experimental data that reflects such a relationship and then examines the agreement between the observations and the results obtained from the model.

In characterizing a given composite, many parameters, such as the elastic constants and volume fractions of the constituents, may be accurately known. Others, such as the bundle and fibre diameters, the fibre strain-to-fail, and the degree of misalignment may also be known or are measurable or estimable. Other information, such as the frictional shear stress may be unknown. Even though the complete data may not be known with precision, the model can be tested by calculating such quantities as the maximum bridging stress S_{max}, the crack opening h_{max} when the

TABLE I Distribution function relationships when $Q(\phi)$ is truncated

Case	$Q(\phi)$	Type	ψ	Failure mode	$f(\theta)$
1	$= 1, \phi < \phi^*$ $= 0, \phi > \phi^*$	Prolate	$\pi/2$	Transverse	$= \cos\theta, \theta > \pi/2 - \phi^*$ $= 0, \theta < \pi/2 - \phi^*$
2	$= 0, \phi > \phi^*$	Prolate	0	Splitting	$= \arcsin\left(\frac{\sin\phi^*}{\cos\theta}\right) \times \cos\theta, \theta > \phi/2 - \phi^*$ $= 0, \theta < \phi/2 - \phi^*$
3	$= 1, \phi > \phi^*$ $= 0, \phi < \phi^*$	Oblate	$\pi/2$	Splitting	$= \cos\theta, \theta < \pi/2 - \theta^*$ $= 0, \theta > \pi/2 - \phi^*$
4	$= 0, \phi < \phi^*$	Oblate	0	Transverse	$= \arcsin\left(\frac{\cos\phi^*}{\cos\theta}\right) \times \cos\theta, \theta > \pi/2 - \phi^*$ $= 0, \theta < \pi/2 - \phi^*$

TABLE II Distribution function relationships when $Q(\phi)$ is continuous

Case	$Q(\phi)$	Type	ψ	Failure mode	$f(\theta)$
5	$= \cos^m\phi$	Prolate	$\pi/2$	Transverse	$= \cos\theta \sin^m\theta$
6	$= \cos^m\phi$	Prolate	0	Splitting	$= \cos^{m+1}\theta$
7	$= (1 - \cos\phi)^m$	Oblate	$\pi/2$	Splitting	$= \cos\theta(1 - \sin\theta)^m$
8	$= (1 - \cos\phi)^m$	Oblate	0	Transverse	$\sim 1 - (1 - \cos\theta)^{m+1}$
9	$= 1, 0 < \phi < \pi/2$	Isotropic	NA	NA	$= \cos\theta, 0 < \theta < \pi/2$

stress reaches S_{max}, and the work of fracture by varying those parameters for which the uncertainty is greatest. Those values giving the best fit with the experimental data can then be assessed as to their reasonableness.

5.1. Results of parametric variations

The calculated effect of the various parameters on the dependence of the bridging stress on displacement of the gripped end of the tensile specimen is given for the example of an experimental continuous carbon fibre/glass matrix composite. The fibre and the glass matrix have Young's moduli of 320 and 90 GPa, respectively. The fibres have a mean radius of 4 μm and their volume fraction is 0.48. Experimental microscopic examination revealed that the fibres are gathered into bundles ~ 65 μm in radius. Because there is little free matrix separating the bundles, the volume fraction of fibres in the bundles is assumed to be 0.5. These values are fixed in all of the trial cases considered below.

The parameters investigated include the fibre-failure strain, the fibre-orientation distribution, the critical shear stress for debonding, and the frictional shear stress. Stress–displacement results are given for both splitting and transverse failure modes. However, the displacement for the transverse failure only considers the elongation of the fibres. It does not yet include the effect of withdrawing the broken fibres from their 'sockets' when fibre failure occurs within the matrix. Hence, the transverse failure curves provide information regarding the displacement at which failures occur, but do not represent the subsequent stress–displacement behaviour.

Fig. 8a and b shows the effect of the failure strain of the fibre on the stress–displacement (S–D) curves for the case of splitting and transverse failure, respectively. In both cases the fibre distribution is considered to be rectangular with a cutoff angle of 10°, and the bond and frictional shear values are 100 MPa and 10 MPa, respectively. The fibre strain levels were 0.01 and 0.02. As expected, the maximum stresses are proportional to the failure strains, and at large displacements the curves shift to higher displacement levels.

Fig. 9a and b reveals the effect of fibre distribution on the S–D curves when the shear values are unchanged from the above values and the failure strain is fixed at 0.01. Rectangular distributions with maximum misalignments of 5° and 10° and a parabolic distribution with a cutoff angle of 10° are studied. Fig. 9a shows that the maximum stress and the shape of the S–D curves at small displacements are markedly affected by the distribution for the case of splitting failure. In the case of transverse bridging, the fibre failure occurs abruptly at very small displacements. Broader fibre distributions tend to shift the S–D curves to higher displacements. There is a suggestion some misalignment may be beneficial in increasing the maximum stress level.

The effect of the frictional stress is given in Fig. 10a and b, fixing the bond shear strength at 300 MPa, the

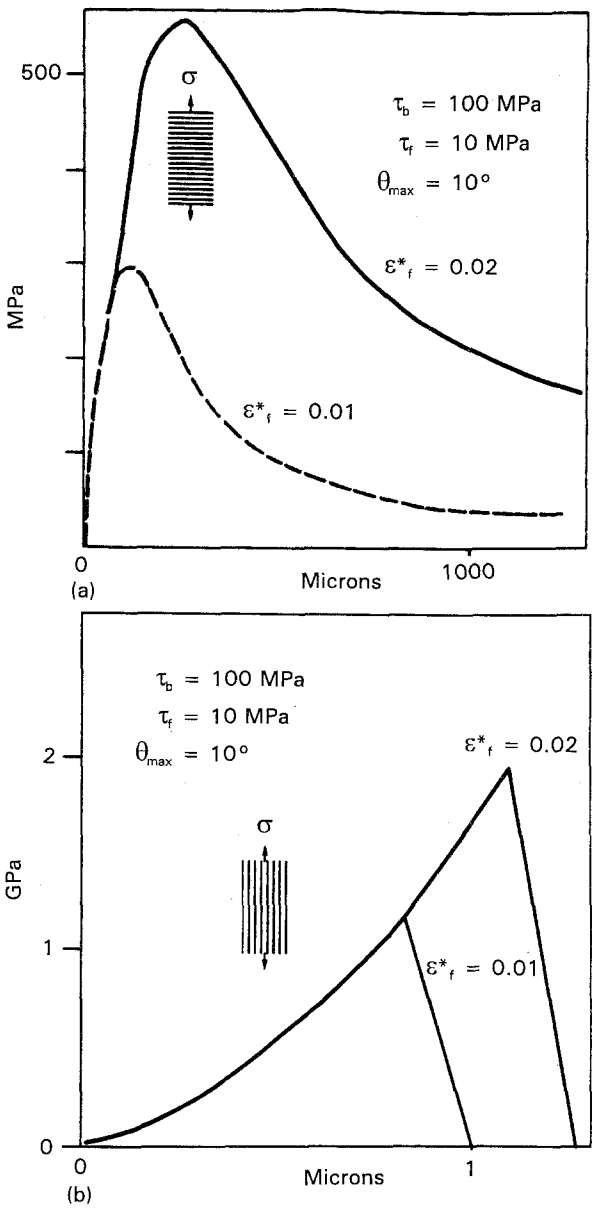

Figure 8 The effect of fibre crack opening resisting stress for the case of a rectangular distribution having a 10° cut-off when the fibre failure strains are 0.01 and 0.02 and when mean fibre direction is (a) normal to the applied stress, or (b) parallel to the applied stress.

fibre failure strain at 0.01, and the fibre distribution to be rectangular with a 5° cutoff angle. The frictional stress levels that were examined are 30 MPa, 3 MPa, and 0.3 MPa. Fig. 10a shows that in the splitting mode the S–D curves become broader and have lower maximum stress values as the frictional shear levels decrease. The decrease in the maximum stress is even more pronounced for transverse cracking, as seen in Fig. 10b. The peak stress when the shear stress is 3 MPa is about half of that when the shear stress is 30 MPa. The curves also shift to higher displacement values.

Finally, the effect of the strength of the shear bond is examined for the case when the frictional stress is fixed at 3 MPa, the other parameters being the same as just discussed. The shear bond values are 300 MPa, 30 MPa, and 3 MPa. Fig. 11a shows that the S–D curve is unchanged for the values 300 MPa and 30 MPa, but a very pronounced change in the shape of

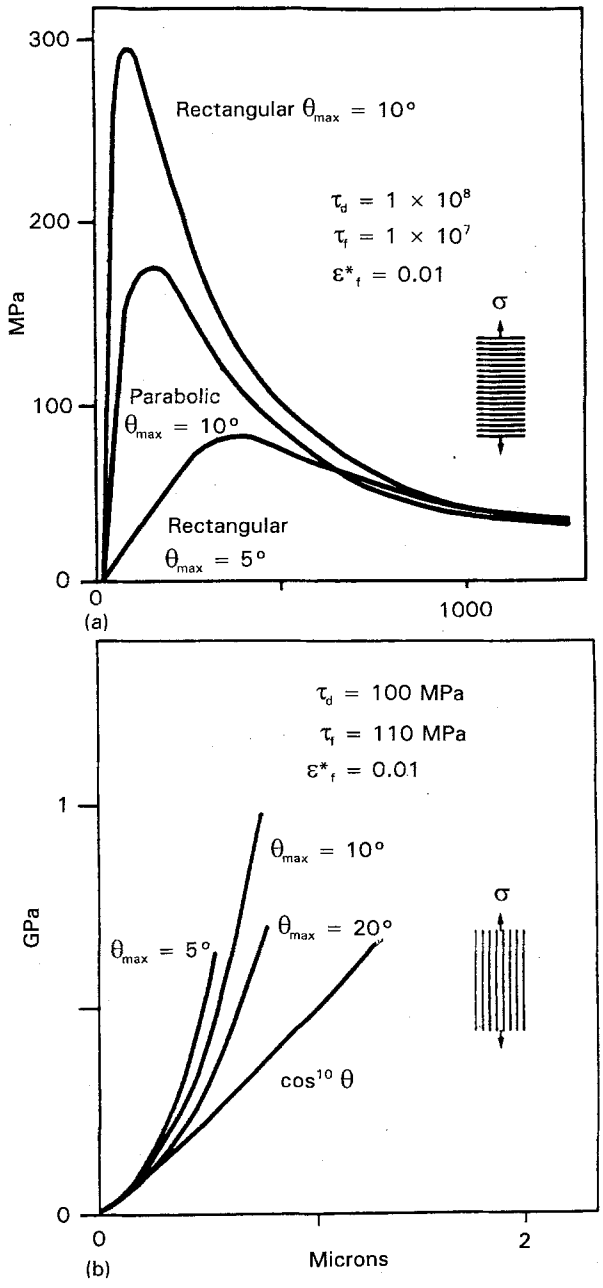

Figure 9 The sensitivity of the crack bridging stress on the degree of fibre misalignment is given for various indicated statistical distributions for cases where the mean fibre direction is (a) normal to the applied stress, or (b) parallel to the applied stress.

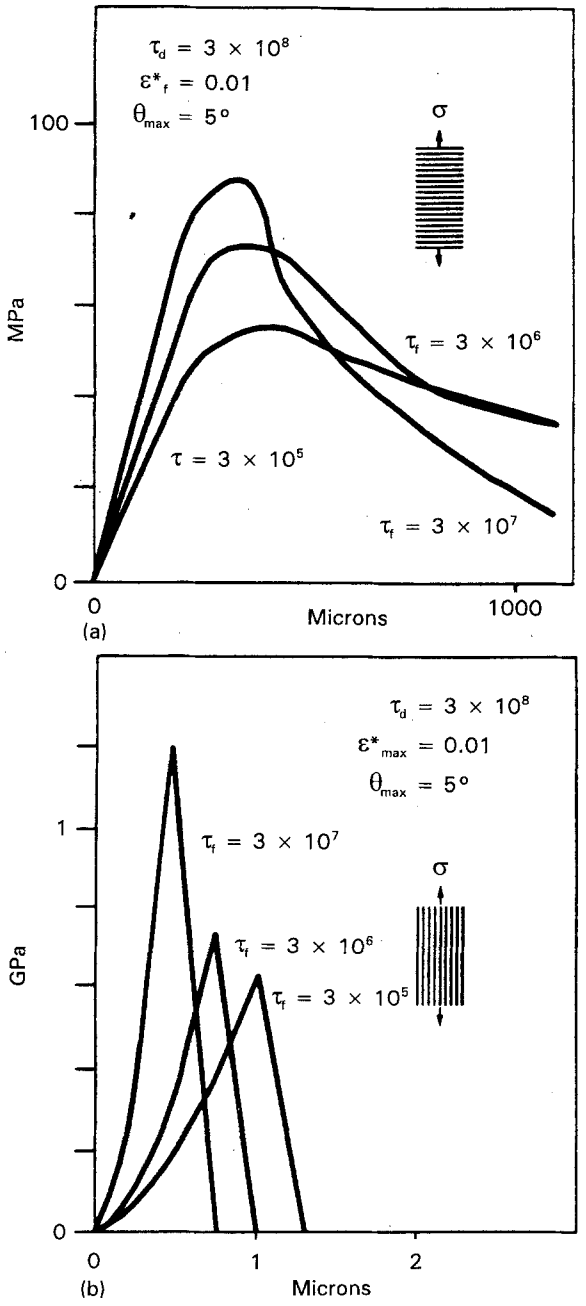

Figure 10 The effect of the fibre–matrix frictional shear stress on the dependence of the bridging stress on the crack opening is shown for the cases where the mean fibre direction is (a) normal to the applied stress, or (b) parallel to the applied stress.

the curve and a lowering of the maximum stress results when the bonding stress is reduced to the level of the frictional sliding shear stress. For the parameters chosen there is little effect on the transverse strength related to the debonding shear strength, as can be seen in Fig. 11b.

In summary, aside from the effect of the fibre strength, the above results indicate that when the fibres run predominantly transversely to the crack face, the frictional shear stress has the greatest effect on the S–D behaviour. However, when the crack runs parallel with the mean direction of the fibres, almost all of the parameters have a significant effect on the S–D curve.

5.2. Comparison with experiment

The most straightforward experimental test of the present model would be to apply unidirectional tension on a composite having a single crack transverse to the stress axis. However, producing a single matrix crack can be achieved in practice more readily, if the specimen is tested in 3-point bending, especially when failure occurs by splitting. Such tests have been performed on glass fibre-reinforced epoxy matrix composites and on graphite fibre-reinforced glass composites [1]. The results from those tests are compared below with the results from the present model.

In many such cases, once the crack forms under continued displacement the two halves of the specimen rotate around the axis of the center load in a hinge-like manner. This behaviour is favoured when the matrix is a hard non-yielding brittle material, and

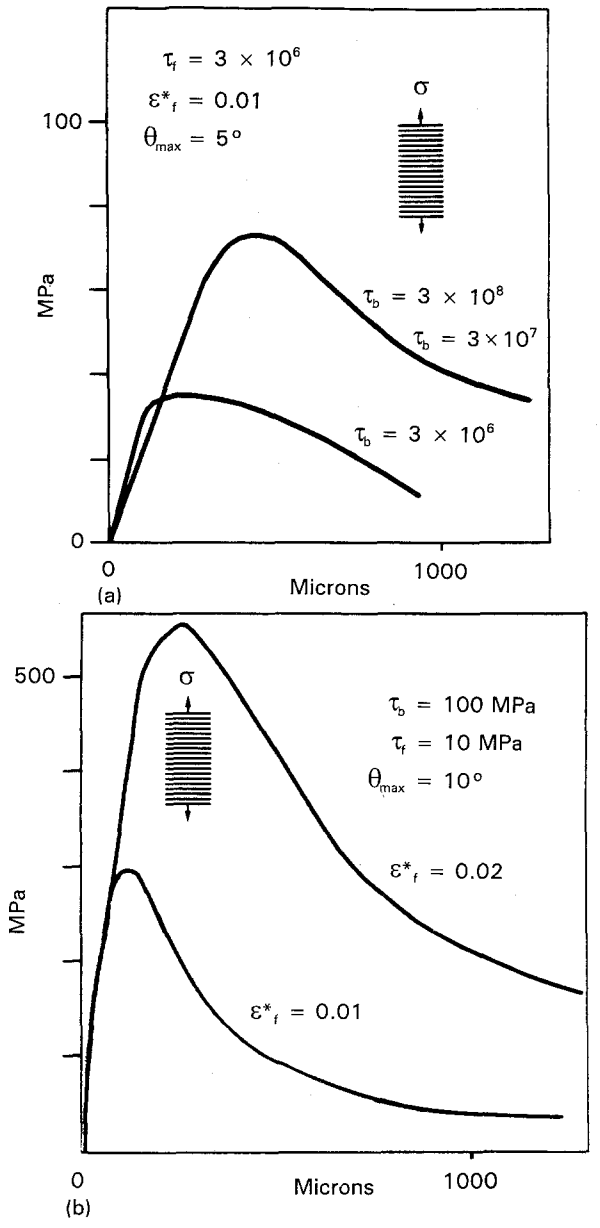

Figure 11 The effect of the fibre–matrix debond shear stress τ_b on the dependence of the bridging stress on the crack opening is shown for the cases where the mean fibre direction is (a) normal to the applied stress, or (b) parallel to the applied stress.

the crack runs parallel to the average direction of the fibres. When such a hinge-like behaviour occurs, the method given in Appendix D relates the applied bending force to the bridging tensile stress at the crack site farthest from the hinge axis. At that location the separation between the crack faces is twice h_f, and from simple geometric considerations is given by

$$2h_f = 4b'z'/L' \tag{41}$$

where L' is the span length, b' the height of the specimen, and z' is the displacement at the center load point. Thus, the tensile stress S can be determined as a function of h_f. The maximum in the calculated stress S_{max} occurs at h_{max}, which is the value of h_f when the applied load is a maximum. In favourable cases S_{max}, h_{max}, and the work of fracture (*WOF*) can be determined. The latter is obtained by integrating S with respect to h_f.

Such a clean hinge-like matrix failure is suppressed if a large fraction of the bundles bridge the crack at large crossing angles. In this case the crack often does not propagate cleanly from the top to the bottom of the bar; multiple cracking and matrix crumbling at the center loading site may also occur. Such bend test data cannot then be reliably converted into equivalent tensile test results. At best, a crude estimate of S_{max} may be inferred using simple beam equations; a similar estimate of *WOF* may be inferred from the load–displacement curve.

Information regarding the crack-bridging stresses at small crack openings may remain hidden when an initially uncracked sample is tested at a constant displacement. A threshold displacement is needed in order to raise the stress level enough to produce [7, 11, 12] the matrix crack. Thus, the crack-bridging stress cannot be directly measured when the displacement is less than the threshold value.

Not all of the values for the parameters needed to calculate the crack opening versus the applied stress dependence may be known, as was the case for the two sets of data given below. Instead, the problem was inverted, i.e. we sought to infer the values of missing data from the "best" fit of the calculated to the experimental observations. Specifically, the data that was missing were the values of τ_d, τ_f, and the degree of misalignment. Furthermore, the bundle size and fibre failure strain were only known approximately.

The procedure for obtaining bounds on the values of these unknown parameters was to estimate initially the bundle size, failure strain, and misalignment cut-off angle. Combinations of τ_d and τ_f were then systematically scanned to search for the minimum overall deviation between the calculated and the observed results. The trial values of τ_d and τ_f that produced the least deviation were then fixed; trial values for the failure strain, bundle size, and cut-off angle were similarly scanned. This complete cycle was then repeated until the deviation of the calculated from the observed results was minimized.

The overall deviation q was defined as the sum of the squares of the relative deviations, i.e.

$$q = \sum_{i=1}^{4} \frac{[M_i(\text{obs.}) - M_i(\text{trial})]^2}{M_i(\text{obs.})M_i(\text{trial})} \tag{42}$$

where M_i represents the measures of interest, e.g. the maximum bridging stress S_{max}, the crack opening when the stress was maximum h_{max}, the crack opening when the stress had dropped to half of the maximum value $S_{0.5}$, and the work of fracture *WOF*.

5.2.1. *Unidirectional graphite fibre-reinforced glass composite*

The detailed specifications of this composite supplied through the kind cooperation of the Corning Glass Works have been previously reported [1], along with the results of its force–displacement behaviour when subjected to a three-point splitting mode test. Only those details relevant to the *a priori* estimation of its fracture response are presented here.

5.2.1.1. Experimental data. The matrix was a borosilicate glass, and the nominal properties of the graphite fibres are diameter 8 μm, Young's modulus 320 GPa, and failure strain 0.58%. The properties of the matrix are Young's modulus 91 GPa, failure strain 0.08%, and Poisson ratio 0.20. The composite contained 48 volume per cent of fibre reinforcement and exhibited a flexural strength of 585 ± 35 MPa and a Young's modulus of ~ 170 GPa.

Chemical dissolution of the matrix glass revealed the fibres to be grouped into bundles having elliptical (0.4 × 1.2 mm) cross sections. Tests on extracted individual graphite filaments gave failure strains of 1.1 ∓ 0.2% when tested over short gauge lengths [13] of the order of 100 fibre diameters. From this scatter in relative strength and from the ratio of the mean failure strains at short gauge lengths relative to the conventional 20 mm gauge length, a Weibull modulus of about 5 for the strength of the filaments was deduced.

The composite was cut into bars for single-edge notched beam testing. The mean direction of the fibres was parallel to the height. The test span was 50.8 mm, the thickness 5.1 mm and the height 22.2 mm. A representative force versus displacement curve is shown in Fig. 12. In duplicate tests the mean maximum load was 313 N at a center bar displacement of 0.10 mm. The work of fracture, as determined from the area under the curve over a displacement range of ten times the displacement at the maximum load, was 470 $J m^{-2}$. After testing the specimens remained loosely bridged by bundles that had not yet failed. Most of the unfailed bundles appeared to lie nearly parallel to the crack plane. This behaviour closely fits the criteria for using the "hinge" model.

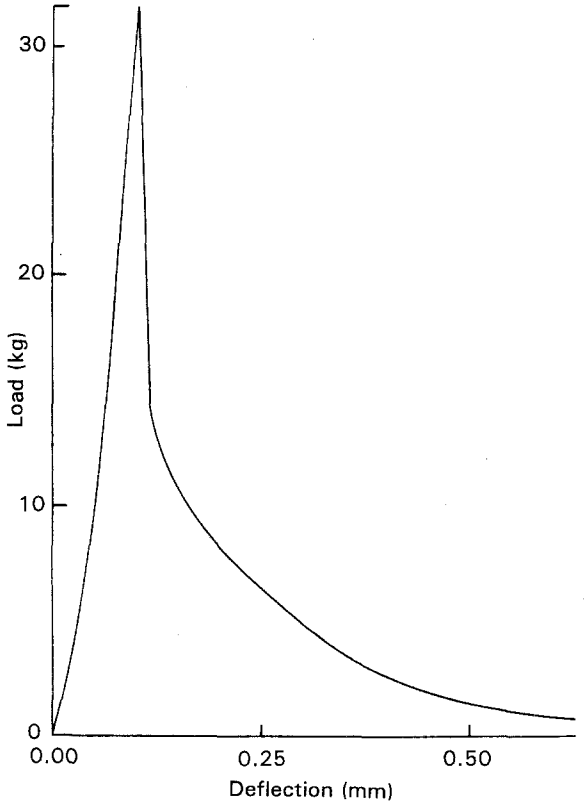

Figure 12 Experimental data for the splitting mode failure of a nominally unidirectional borosilicate glass matrix composite reinforced with 45 volume per cent of graphite fibre.

The "hinge" model (see Appendix D) gives the inferred maximum bridging stress, after the occurrence of matrix cracking, to be 1.9 MPa at a separation between the crack faces of 40 μm. The stress drops to half of the maximum value at a crack opening of 190 μm.

In a second experiment, specimens of the same composite were cut into bars with the fibres parallel to the long axis. Four bars 2.92 mm in height were tested in a 3-point bend mode over a 25 mm test span. The mean breaking stress derived from elementary strength of material equations was 445 ± 25 MPa, and the work of fracture was 80 ± 20 $kJ m^{-2}$. Unfortunately, extensive buckling occurred on the compressive side of the test bar, invalidating the use of Appendix D to translate the experimental results into "equivalent" tensile test data.

5.2.1.2. Inferred parametric values. Most of the required physical and mechanical properties of the constituents, including the fibre failure strain, fibre bundle size, and fibre orientation, were approximately known; but there was no *a priori* information regarding the values of τ_d or τ_f. For simplicity, a rectangular distribution of fibre orientations was assumed. The fact that the large elliptical bundles were comprised of a subset of smaller bundles introduced some ambiguity regarding which was the appropriate bundle size. Both sizes were considered in seeking which gave the best fit to the data.

The data for the splitting mode of failure could be fitted with values of q ranging from 0.9 to 1.7 by varying the cut-off for the crossing angle, the shear strengths for debonding and frictional slippage, as well as the fibre failure strains over narrow ranges, as shown in Table III.

The constancy of the calculated crack opening h_{max} corresponding to the maximum in the resisting stress S_{max} is an artifact caused by the discreteness of the steps in the computer code by which the crack is opened. The increments in the opening corresponded to 15% of the previous opening. The input parameters were scanned similarly in discrete increments, e.g. 0.5° for the cut-off angle, 0.0005 for the fibre failure strain, and a factor of 1.8 for increases of τ_d and τ_f. Assuming that the small sub-bundles were the crack bridging entities resulted in calculated values for the fracture data that were in gross disagreement with the experimental values. However, assuming that the bundles were 0.4 × 1.2 mm, which is the measured size given above, the results shown in Table III were obtained.

5.2.2. Unidirectional E-glass fibre-reinforced epoxy

This composite was also reported previously [1] and consisted of 0.6 volume fraction of nominally parallel multifilament strands of 10 μm diameter E-glass filaments in an epoxy matrix. Because the composite was produced by pultrusion, the strands were expected to be nearly parallel. Microscopic examination showed that the strands were about 1.2 mm in diameter, but appeared to be made up of bundles about 0.2 mm in diameter. The Young's modulus of the

TABLE III Comparison between experimental results for splitting failure of a graphite fibre/borosilicate glass composite and the computed expected results

Input parameters				Fracture data		
ϕ	ε^*	τ_d (MPa)	τ_f (MPa)	h_{max} (μm)	S_{max} (MPa)	WOF ($J\,m^{-2}$)
Experimental						
	0.011 ± 0.002			40	1.9	470
Computed						
6	0.0125	10	3	65	0.7	470
6	0.0130	10	3	65	0.7	730
6	0.0135	10	3	65	0.7	750
6.5	0.0115	10	3	50	0.8	560
6.5	0.0115	10	6	50	0.8	370
6.5	0.012	10	3	50	0.8	580
7	0.011	10	3	39	0.8	510

TABLE IV Comparison of calculated versus observed results for an E-glass fibre-reinforced epoxy composite tested in splitting mode

Input parameters				Results		
ϕ	ε^*	τ_d (MPa)	τ_f (MPa)	h_{max} (μm)	S_{max} (MPa)	WOF ($kJ\,m^{-2}$)
Experimental values						
				150	3.8	1.15
Values calculated from model						
8	0.024	16	13	245	3.8	2.17
8	0.024	25	13	245	3.1	1.76
8	0.024	25	20	195	3.2	1.40
8	0.0235	25	20	195	3.2	1.32
7.5	0.024	25	20	195	2.5	1.20

fibres is 70 GPa and of the resin was estimated to be 1.7 GPa. The failure strain of the glass fibres was not known, but values in the range 0.02–0.03 are expected.

The test bar was subjected to a 3-point loading at a span length of 75 mm. The bar was 19 mm in height and was notched to a depth of 1.9 mm at the midspan. The fibre orientation was parallel to the height, so that failure corresponded to the splitting mode. The force dropped discontinuously from a maximum value of 141 N (Newtons) to 101 N and then increased again to a second maximum of 103 N at a center beam displacement of 0.20 mm. Using the deconvolution procedure given in Appendix D indicates that S_{max} is 3.8 MPa, h_{max} is 150 μm, and WOF is $1150\,J\,m^{-2}$.

The values of the parameters leading to the best fits to the data are given in Table IV, based on a bundle size fixed at 0.2 mm diameter.

6. Summary and concluding remarks

This paper proposes that (1) even nominally unidirectional arrays of reinforcing fibres are typically comprised of groupings (bundles) of parallel fibres, (2) these bundles can behave as if they were larger diameter reinforcements, (3) the spatial orientation of bundles generally deviates statistically from the nominal mean direction, (4) bundles that cross the crack plane at an angle other than normal or parallel to the plane must flex as the crack opens, and (5) the components of bridging force that resist crack opening arise from stretching of the fibre bundle and from bending of the bundle.

In other respects the composite is modelled in the usual way, except that the misorientation may affect certain details. The fibres and bundles are assumed to be adhesively bonded to the matrix, requiring a characteristic threshold shear stress to be applied at the interface in order to cause debonding. Once debonded, slippage of the bundle relative to the matrix is allowed. Such slippage is assumed to be resisted by a fixed characteristic interfacial frictional shear stress. The fibres fail at a strain level dependent on the length over which the fibre is debonded, in accordance with expectations based on Weibull statistics. The contribution of pullout is explicitly considered in the case of fibres having discrete lengths and is estimated using Weibull statistics for the case of continuous fibres, using the model previously given by Sutcu [14].

Ideally, in order to test this theoretical model the values of the parameters must be known independently. In addition, measurements of the crack opening as a function of an applied tensile test are required. Such complete information is not available at this time. However, some related 3-point bend test measurements have been made, which in favourable cases can be manipulated to yield the underlying response under pure tensile test conditions.

By adjusting the values of those parameters that were not independently known, it was possible to obtain an approximate fit to the experimental data obtained on a carbon fibre/borosilicate glass composite as well as on a E glass/epoxy composite. By this means the missing values could be inferred. The results obtained in this way appear to be physically reasonable.

Perfect fits within experimental and/or computational error were not obtained. In particular, the maximum fibre-crossing angle for best fit was greater than expected from comparison with the actual specimen. One possible reason is that the present model assumes that the fibre bundles are free to act as independent

cantilevers. In a densely packed composite the bundles are likely to interfere with the flexural response of adjacent bundles. As a result, the neighbouring fibres will provide mechanical support to any given bundles, especially in the region where the bundle emerges from the crack face. Hence, the model underestimates the flexural stiffness and probably also the tensile strain in the crack-bridging region. Computationally, such an underestimate can be compensated by an increase in the bundle-crossing angle.

In addition to providing a basis for calculating the ultimate crack bridging strength and *WOF*, modelling the dependence of the bridging stress on the crack opening should be useful in treating finite cracks in which the crack opening varies with distance from the matrix crack tip, and the crack opening in turn depends on the bridging stress.

Finally, it is hoped that this comprehensive model provides insight into the behaviour of imperfect composites. Undoubtedly, as more data and observations of the fracture process become available, additional phenomena must be included. Such work is essential for testing the validity of the proposed concepts.

Appendix A. Stress and displacements for simple concentric cylinder systems

Some results presented through Section A1, have been previously given (e.g. [5, 6]), but are summarized here for ready reference.

Consider a unidirectional composite containing v_f volume fraction of fibres, which is subjected to a uniaxial tensile stress S parallel to the fibres and a corresponding strain $e_c(\infty) = S/E_c$. (E_c is the Young's modulus of the composite in the fibre direction.) Let the ends of the fibres emerge from a free surface, such as in the case of a transverse matrix crack bridged by the fibre. Force balance requires that the emerging fibres carry a stress S/v_f, which is progressively transferred to the matrix with increasing distance x from the free surface.

Correspondingly, the strain in the fibres progressively decreases from $\varepsilon_f(0)$ at $x = 0$ to the background strain $\varepsilon_f(\infty)$. The deviation of the strains in the fibres and in the matrix from the background strain results in a net displacement u of the fibres relative to the matrix at the free surface. That is

$$u = \int_0^\infty \{[\varepsilon_f(x) - \varepsilon_f(\infty)] - [\varepsilon_m(x) - \varepsilon_m(\infty)]\}\,dx = \int_0^\infty [\varepsilon_f(x) - \varepsilon_m(x)]\,dx \quad \text{(A1)}$$

The quantity $\varepsilon_f(x) - \varepsilon_f(\infty)$ is the departure of the fibre strain from its value far from the free surface and will be abbreviated to $\eta_f(x)$. Force balance requires that the fibre and matrix mean stresses $s_f(x)$ and $s_m(x)$ obey

$$s_f(x)v_f + s_m(x)v_m = S \quad \text{(A2)}$$

This condition in turn relates $\varepsilon_m(x)$ to $\varepsilon_f(x)$ and leads to

$$u = (E_c/v_m E_m)u_f \quad \text{(A3)}$$

The incremental elongation of the fibre u at the free surface (crack face) relative to that at the same location had the composite remained crack-free is

$$u_f = \int_0^\infty \eta_f(x)\,dx \quad \text{(A4)}$$

A.1. Fibres coherent with matrix

The difference between the fibre tensile strain near the crack and that far distant, when the fibre is coherently bonded to the matrix, is given by

$$d^2\eta(x)/dx^2 = k^2\eta(x) \quad \text{(A5a)}$$

For infinitely long fibres the solution

$$\eta(x) = \eta(0)\exp(-kx) \quad \text{(A5b)}$$

is applicable to the cases of load transfer between a broken fibre and an unbroken matrix or between a cracked matrix and an intact fibre. All models consider the fibres to be concentrically surrounded by the matrix. The relative radii of the fibres and the matrix are defined by the volume fractions of these two constituents. The case of the broken fibres was first treated by Cox [13]. The inverse case, in which intact fibres bridge a matrix crack, is discussed next.

The BHE [7] model assumes a shear stress dependence in the matrix given by

$$\tau_m(r, x)/\tau(a, x) = (v_f/v_m)(R^2 - r^2)/ar \quad \text{(A6a)}$$

where τ_m is the shear stress in the matrix, $\tau(a, x)$ is the shear stress at the fibre–matrix interface, r is radial distance and R is the outer cylindrical radius defined through $v_f = (a/R)^2$.

This dependence satisfies the boundary conditions, namely at $r = a$, the matrix shear stress matches the fibre shear stress, at $r = R$, the matrix shear stress vanishes, and at all values of r force equilibrium is maintained. The model leads to a tensile stress in the matrix that is independent of radial distance r. The results are then translated in terms of another simpler, but energetically equivalent, model. The computed value of the exponential decay constant is

$$k = k_1 = \left[\left(\frac{G_m}{E_f} + \frac{v_f}{v_m}\right)\Big/(1 + v_m)\ln\left(\sqrt{\frac{R'}{a}}\right)\right]\Big/a \quad \text{(A6b)}$$

in which R' is a mean effective matrix radius given by

$$\ln\left(\frac{R'}{a}\right) = -(2\ln v_f + v_m(3 - v_f))/4v_m^2 \quad \text{(A6c)}$$

I offer an alternative model, which in addition requires that the matrix axial strain at $r = a$ is constrained to match that in the fibre. The local shear stress field around a given fibre is approximated by the three parameter law in which p is an abbreviation for r/R

$$\tau_m(r, x)/\tau(x) = c_0 \ln p + c_1/p + c_2/p^2 \quad \text{(A7)}$$

and where the coefficients also satisfy the conditions used in the preceding model. The resultant values of the coefficients are

$$c_0 = [1 + 2(E_m/E_f)]/[1 - p + (2 - p)\ln p] \quad \text{(A8a)}$$

$$c_1 = \{1 + [1-2(E_m/E_f)]\ln p\}/ [1 - p + (2 - p)\ln p] \quad \text{(A8b)}$$

and

$$c_2 = -c_1$$

leading to the result

$$k = k_2 = \left[\frac{(E_m/E_f)p - (c_0 + c_1)p^2/2}{(1 + \nu_m)(c_0 j_0 + c_1 j_1)}\right]\Big/a \quad \text{(A8c)}$$

in which $j_0 = p(1 + \ln p) - 1$ and $j_1 = 1 - 1/p + \ln p$.

The greatest difference between k_1 and k_2 is only 35%, which occurs when $E_m/E_f = 1$ at $v_f \sim 0.1$. Arguably, k_2 should give a better approximation to the geometric decay of shear stress, inasmuch as the matrix and fibre strains at $r = a$ are forced to be in registry. However, both models are one-dimensional approximations to a two-dimensional problem. Because the two models are in good agreement, and because the expression for k_1 is simpler, we use k_1 when explicit evaluation of k is required.

The functional dependencies of the fibre displacement u at $x = 0$ and the interfacial shear stress $\tau(x)$ do not depend on the specific values of k. The displacement u is

$$u_f = \eta(0)/k \quad \text{(A9a)}$$

The interfacial shear stress $\tau(x)$ is given through

$$\tau = aE_f(d\varepsilon_f/dx)/2$$

or

$$\tau(0) = kaE_f\eta(0)/2 \quad \text{(A9b)}$$

If we assume that debonding initiates when $\tau_0 = \tau_d$, where τ_d is a material parameter, then

$$\eta^* = 2\tau_d/kaE_f \quad \text{(A10a)}$$

and

$$u_f^* = 2\tau_d/k^2aE_f \quad \eta^*(0)/k \quad \text{(A10b)}$$

where η^* is an abbreviation for $\eta^*(0)$; η^* and u_f^* are critical strain and displacement parameters that define the onset of debonding at the fibre wall, unless the fibre breaking strain intercedes before Equation A9 can be satisfied.

A2. Loss of coherence of continuous fibre bundles

In the slipped region the fibre stress and strain as a function of distance x from the crack face and the frictional shear stress τ_f are given by

$$s_f(x) = s_f(0) - 2\tau_f x/a \quad \text{(A11a)}$$

from which one can obtain

$$\eta(x) = \eta(0) - (2\tau_f/aE_f)x = \eta(0) - Cx \quad \text{(A11b)}$$

the abbreviation C being definable by inspection. Let the value of x at the boundary between the bonded and the debonded regions, where $\eta(x) = \eta^*$, be designated L', which is then given by

$$L' = [\eta(0) - \eta^*]/C \quad \text{(A12)}$$

For values of $x > L'$, let $x = L' + z$. Then

$$\eta(x) = \eta^*\exp(-kz) \quad \text{(A13)}$$

from which the elongation in the slipped region is obtainable as

$$u_{f,s} = [\eta^2(0) - \eta^{*2}]/2C \quad \text{(A14)}$$

The elongation over the range $x > L'$ must be added to $u_{f,s}$ to give the total elongation u_f, i.e.

$$u_f = u_{f,s} + \eta^*/k \quad \text{(A15)}$$

However, once slippage initiates, the relative contribution of the coherent region to the total elongation becomes negligible.

A3. Loss of coherence of discontinuous fibre bundles

We now consider a bridging discontinuous fibre bundle. Let its nearest end to the crack plane, as measured along its axis, lie a distance $L_{f,i}$ from the crack plane. The distance along the fibre relative to the crack face is designated by x, as shown schematically in Fig. 6. If fibre pullout occurs, then the end of the fibre moves from its original position. The new position can be calculated as follows.

Let the length of the bundle that spans the open crack from the crack plane to the crack face be L. Then the length of the embedded fibre to the nearest end is $X = L_{f,i} - L$. Let the length of the debonded region of the fibre be L_s. We first treat the simple case in which there is only frictional coupling between the fibre and the matrix. Later we examine how adhesive bonding modifies the pullout process.

A3.1. No fibre–matrix bonding

In the absence of fibre–matrix bonding, the axial stress at the embedded end of the fibre is zero. Thus, there is a small region in which the fibre strain is less than the applied strain $\varepsilon(\infty)$, i.e. in which $\eta < 0$. We shall neglect this effect and simply set η equal to zero at the fibre end. Equations A10a and A10b remain valid if τ_f replaces τ_d, because slippage can only occur if $\tau(0)$ exceeds τ_f. In accordance with Equation 12, the length L' of the slipped region increases with increasing $\eta(0)$ until $L' = L_{f,i} = X_i$, which defines the onset of pullout. Any further increase of the crack opening causes X_i to diminish. Thus, using Equation A12 the maximum value of $\eta(0)$ is $CL_{f,i}$. As the crack opens further $\eta(0)$ is given by CX_i, and $\eta(x)$ is simply

$$\eta(x) = C(X_i - x) \quad \text{(A16a)}$$

where X_i is related to $L_{f,i}$ and L through

$$X_i = L_{f,i} - L + \int_0^{X_i} \eta(x)\,dx \quad \text{(A16b)}$$

A3.2. Fibres initially bonded to the matrix

When the fibres are initially adhesively bonded to the matrix, the shear stress level must reach τ_d to initiate debonding. In accordance with Equation 10b, this condition is satisfied when $L > u_f^*$. We first consider the case in which the fibre end is free of the matrix. The demarcation between the bond and the debonded regions is termed the Fibre–Matrix Debond Site (FMDS), as shown in Fig. 6.

Once debonding has commenced, the fibre strain decreases linearly with distance x from the crack face according to

$$\eta(x) - \eta(L_s) = C(L_s - x) \quad \text{for } x < L_s \quad \text{(A17)}$$

where L_s is the value of x at the FMDS, and $\eta(L_s)$ is the fibre strain at the FMDS which satisfies the debonding condition. For $x > L_s$, $\eta(x)$ is governed by Equation A5a. Introducing the boundary conditions $\tau(x = L_s) = \tau_d$ and $\eta(L_{f,i}) = 0$, leads to

$$\eta(L_s) = 2\tau_d \tanh(kZ)/(ka\,E_f) \quad \text{(A18)}$$

where Z is an abbreviation for $L_{f,i} - L_s$. Thus, as the FMDS approaches the end of the fibre, $\eta(L_s)$ vanishes, so that the condition for the onset of fibre pullout is the same as if the fibre had been initially debonded, although the stress needed to initiate frictional sliding is greater.

We now consider the case in which the end of the fibre is bonded to the matrix. A tensile stress s_{end}^* at the end of the fibre is postulated to be required for end debonding, i.e. $\eta(L_{f,i}) = s_{end}^*/E_f = \eta^*$. Introducing this boundary condition into Equation 5a leads to

$$\eta(L_s) = \eta^*/\cosh(kZ) + 2\tau_d \tanh(kZ)/(ka\,E_f) \quad \text{(A19)}$$

This relationship indicates that as L_s approaches $L_{f,i}$, $\eta(L_s)$ increases and approaches η^*. Introducing this into Equation A17 indicates that $\eta(0)$ just prior to pullout is greater by the increment η^* than is the case for no end bonding. However, once the end bond is broken, then the $\eta(0)$ value must drop discontinuously to the value given by Equation A17.

Appendix B. Estimation of the dependence of h_m on h_f

In misaligned composites the stress and strain fields of one fibre will be perturbed by the presence of its non-parallel neighbours. Hence, the conditions for static equilibrium throughout the composite cannot be as simply expressed as by Equation A2 in Appendix A, which refers to a unidirectional composite with the fibres normal to the applied stress and perpendicular to the crack. Furthermore, in such an idealized composite, the fibre orientations also coincide with the direction of the principal Young's modulus of the composite. These simplifications allow the displacements of the fibre and the matrix to be determined in a straightforward manner.

This Appendix B offers an approximate model for the displacement of the matrix at the crack face when the reinforcing fibres are misaligned. The assumptions are: (1) the normal to the crack is an axis of rotational elastic symmetry; (2) the response of the composite can be synthesized from the separate responses of unidirectional composites in which the fibres are inclined as they cross the fracture plane; (3) the weighting functions are the same as those that describe the composite microstructure; and (4) the elastic constants used in assumption (2) are those of the composite as a whole.

The elastic properties of a fibre-reinforced composite are dependent on the fibre orientation. Although the stiffness of the matrix can vary due to locally varying triaxial constraints, we treat the matrix as elastically isotropic and unaffected by being in the composite. Accordingly, we arbitrarily ascribe the orientational dependence of the Young's modulus E_c for the composite on an orientational dependence of $E_{f,eff}$, the "effective Young's modulus" of the fibres through

$$E_c = v_f E_{f,eff} + v_m E_m \quad \text{(B1)}$$

where E_c is the Young's modulus of the composite when the fibres are oriented at the angle θ relative to the crack plane. The uniaxially applied traction is taken to be normal to the crack plane. This modulus may be given by an appropriate model or may be experimentally determined.

In the expressions below, S, u, v, and E have their usual meanings, as do the subscripts f, m, and c; x is distance from the crack face. Quantities measured normal to the crack plane are primed, whereas those parallel to the fibre axis are left unprimed.

Consider first an unidirectional composite in which the fibres (bundles) are inclined at the angle θ relative to the crack plane. The area fraction of the fibres at the crack face is the same as v_f for the overall composite. Static equilibrium requires that in the direction normal to the crack face

$$v_f S_f'(x) + v_m S_m'(x) = S_c' \quad \text{(B2a)}$$

Similarly, in the direction parallel to the fibres

$$v_f S_f(x) + v_m S(x) = S_c \quad \text{(B2b)}$$

For simplicity we assume proportionality between the macroscopic stresses and strains in the composite normal to the crack plane, as well as between the local stresses and strains of the constituents parallel to the fibre. Thus, Equations B2 and B3, respectively, can be expressed as

$$v_f E_f' \varepsilon_f'(x) + E_m' v_m \varepsilon_m'(x) = E_c' \varepsilon_c \quad \text{(B3a)}$$

and

$$v_f E_f \cdot \varepsilon_f(x) + E_m v_m \varepsilon_m(x) = E_c \varepsilon_c \quad \text{(B3b)}$$

Continuity requires that far from the crack $\varepsilon_f(\infty) = \varepsilon_m(\infty) = \varepsilon_c$ and $\varepsilon_f'(\infty) = \varepsilon_m'(\infty) = \varepsilon_c'$. From these equalities it follows

$$v_f E_f' + v_m E_m' = E_c' \quad \text{(B4a)}$$

and

$$v_f E_f + v_m E_m = E_c \quad \text{(B4b)}$$

Equation B4b represents the simple rule of mixtures inasmuch as the stress S is parallel to the fibres; E_f and E_m represent the usual material constants. However, the situation is different in the case of Equation B4a.

Recalling that E_m is postulated to be isotropic and constant gives $E'_m = E_m$. The composite modulus E'_c is a strong function of the fibre orientation relative to that of the applied stress S'. Approximate expressions for this dependence have been given [15]. We reconcile the orientation dependence in Equation B4a by interpreting E'_f as a direction-dependent material constant such that the equation is obeyed. That is,

$$E'_f = (E'_c(\theta) - v_m E_m)/v_f = E_{f,\text{eff}} \quad \text{(B5)}$$

In order to relate h_m to h_f, it is necessary to translate the various strains to corresponding displacements. Making use of the equality of the strains far from the crack, one can write

$$v_f E'_f(\theta)(e'_f(x) - e'_f(\infty)) + v_m E_m(e'_m(x) - e'_m(\infty)) = 0 \quad \text{(B6)}$$

Integration with respect to x from 0 to ∞ leads to

$$u'_m = -(v_f E'_f(\theta)/v_m)u'_f \quad \text{(B7)}$$

in which u'_m is the contractive displacement of the matrix at the crack face normal to the crack, i.e. h_m. Correspondingly u'_f is the extension of the fibre within the matrix resolved normal to the crack, or $u'_f = U \sin\theta$, where U is the extension in the direction of the fibre. In Equation 13 it was shown that $U = h_f \sin\theta$.

Thus,

$$(h_m/h_f)_\theta = -(v_f E'_f(\theta)/v_m)\sin^2\theta \quad \text{(B8)}$$

Finally, we postulate

$$h_m/h_f = \langle h_m/h_f \rangle = \frac{\int_0^{\pi/2} (h_m/h_f)_\theta Z(\theta)\,d\theta}{\int_0^{\pi/2} Z(\theta)\,d\theta} \quad \text{(B9)}$$

in which $Z(\theta)$ is the weighting function for the number of bundles crossing a unit area of crack surface at the angle θ, as discussed in Section 4.1. Inasmuch as h_f is an independent variable, the above equation allows h_m and h to be determined.

Appendix C. Relationship between misalignment angle ϕ and crack crossing angle θ

Consider a population of fibres that is distributed symmetrically around an axis that represents the mean direction of the overall population. The distribution can be considered in terms of a projection onto a spherical shell in which the axis is a ray emanating from the center of the sphere onto the surface. The center of the sphere coincides with the origin of a three-dimensional Cartesian coordinate system with axes X, Y, and Z. The orientation of the individual fibres can also be represented by rays that intersect the spherical surface. The angular deviations of the individual fibres from the axis are characterized by the cone angle ϕ with respect to the axis. The crack plane and the XY plane coincide. The angle that the axis makes with respect to the crack plane is ψ, and the angle that the fibres make in crossing the crack plane is ϕ. The various fibre distributions are defined as follows:

$Q(\phi)$ = number density of fibres projected on the spherical shell per unit solid angle at angle ϕ from the axis of symmetry:

$P(\phi)$ = total number density of fibres that deviate from the axis of symmetry by an angle ϕ, $P(\phi) = Q(\phi)\sin\phi$;

$f(\phi)$ = number density of fibres that cross the fracture plane at an angle ϕ.

When $\psi = 0$, the axis of symmetry lies in the XY fracture plane, and we arbitrarily set that axis to coincide with the X-axis. When $\psi = \pi/2$, the axis of symmetry is normal to the fracture plane and coincides with the Z-axis. We discuss this simpler case of $\psi = \pi/2$ next.

C1. Axis of symmetry normal to crack plane

Fibres crossing the fracture (XY) plane at a given angle θ lie represented by a cone produced by rotating a line about the Z-axis inclined at the angle ϕ to the XY plane. Hence, when $\psi = \pi/2$, $\theta = \pi/2 - \theta$, i.e. $\phi = \pi/2 - \theta$, so that $f(\phi)$ is simply

$$f(\phi) = P(\pi/2 - \theta) \quad \text{(C1)}$$

C2. Axis of symmetry lying in crack plane

When the axis of symmetry does not coincide with the axis that defines θ, the translation from $Q(\phi)$ to $f(\theta)$ requires the integration of Q over the surface of the sphere at constant crossing angle θ. Consider a surface area element defined by the spherical bands between θ and $\theta + d\theta$ around the Z axis, and by ϕ and $\phi + d\phi$ around the X axis. This element is given by

$$dA = \frac{\sin\theta \sin\phi\, d\theta\, d\phi}{\sqrt{(1 - \cos^2\phi - \cos^2\theta}} \quad \text{(C2)}$$

Because of symmetry it is sufficient to consider only 1 octant of the sphere.

The total number N of misaligned fibres can be determined directly by integrating $Q(\phi)$ over the hemisphere defined by varying ϕ from 0 to $\pi/2$, i.e.

$$N = 2\pi \int_0^{\pi/2} Q(\phi)\sin\phi\, d\phi \quad \text{(C3)}$$

This quantity must be the same as by integrating $Q(\phi)$ over the 4 octants that comprise the hemisphere defined by varying θ from 0 to $\pi/2$, i.e.

$$N = 4\int_0^{\pi/2} \cos\theta \int_{\pi/2-\theta}^{\pi/2} \frac{Q(\phi)\sin\phi\, d\phi}{\sqrt{\cos^2\phi - \cos^2\theta}} \quad \text{(C4)}$$

Note that integrating first with respect to θ leads to C3.

By inspection it can be seen that $f(\theta)$ is given by the quantity within the curly brackets, i.e.

$$N = \int_0^{\pi/2} f(\theta)\, d\theta \quad \text{(C5)}$$

C3. Normalization of distribution functions

The area on the crack plane intercepted by a fibre (or bundle) of radius a when it traverses the crack plane at

the angle θ is $\pi a^2/\sin\theta$. Thus the area intercepted by all fibres at that angle is proportional to $f(\theta)/\sin\theta$. The total area intercepted by all fibres of all orientations is v times a unit area, where v is the volume fraction of fibres in the composite. That is,

$$K\pi a^2 \int_0^{\pi/2} \frac{f(\theta)\,d\theta}{\sin\theta} = v \qquad (C6)$$

where K is a normalizing constant to be determined from this expression. The actual number of fibres (or bundles) crossing the crack plane at $\theta \pm d\theta$ is $Kf(\theta)$. The normalized value of $Q(\phi)$ or $P(\phi)$ can be determined similarly.

Appendix D. Approximate procedure for translating bend test data into "equivalent" tensile test data for the case of the splitting failure mode

The following simple model translates the main features of experimental 3-point bend test measurements into equivalent tensile test results. The quantities of particular interest are the maximum stress supportable by the bridging bundles and the spacing h corresponding to the maximum stress. We assume that in failing, the bend test specimen acts like a hinge. That is, the matrix is assumed to be completely cracked, and the two halves of the specimen, held together by the bridging fibre bundles, are considered to be rigid blocks that pivot around the top of the crack, at which point the center load acts. The crack face separation increases linearly with increasing distance from the pivot. At any given distance, the crack face separation increases with increasing downward displacement of the center load site.

The magnitude of the crack opening is readily determined using simple geometry. For a test specimen having a span of length L, height B, thickness C, and center load point deflection d, the crack opening h as a function of distance Y from the pivot is simply

$$h(d, Y) = 2dY/L \qquad (D1)$$

The load P at the centre of the bar is given by equating moments around the pivot and is

$$P = \frac{4C}{L}\int_0^B YS\,dY \qquad (D2)$$

in which S is the stress to be determined. By change of variable, using Equation D1 yields

$$P = \frac{CL}{d^2}\int_0^{h_{max}} hS\,dh \qquad (D3)$$

which upon differentiation with respect to d and some manipulation gives

$$P' = dP/dd = -2P/d + 4B^2CS/Ld \qquad (D4)$$

and

$$S(h_{max}) = L(P'd + 2P)/4CB^2 \qquad (D5)$$

Thus, from the measured load, deflection, and the slope of the load with respect to the center point deflection, the stress as a function of crack opening can be calculated. Because at the maximum applied load, $P = 0$, the maximum stress occurs at the same deflection as the maximum in the load. By noting geometric similitude it follows that

$$h_{max} = 2dB/L \qquad (D6)$$

Acknowledgements

The help of Ms Paula Breslin and Mr David Raycroft in the preparation of the manuscript is acknowledged with pleasure and appreciation. The discussions with Drs David Duquette, Demitri Lagoudas, and Muzaffer Sutcu were very helpful and are much appreciated.

References

1. W. B. HILLIG, *J. Mater. Sci.* **29** (1993) 419.
2. J. MORTON and G. W. GROVES, *J. Mater. Sci.* **9** (1974) 1436.
3. M. R. PIGGOTT, in "Load bearing fibre composites" (Pergamon Press, New York, 1980) p. 133.
4. M. HETENYI, in "Beams on elastic foundation" (University of Michigan Press, Ann Arbor, MI, 1948) p. 10.
5. W. B. HILLIG, *Ceram. Bull.* **66** (1987) 373.
6. M. SUTCU and W. B. HILLIG, *Acta Metall. Mater.* **38** (1990) 2653.
7. B. BUDIANSKI, J. W. HUTCHINSON and A. G. EVANS, *J. Mech. Phys. Solids* **34** (1986) 167.
8. G. A. COOPER, *J. Mater. Sci.* **5** (1970) 645.
9. R. M. JONES, in "Mechanics of composite materials" (Hemisphere Publishing Corp., New York, 1975) p. 31.
10. G. S. WATSON, *J. Geol.* **174**, 5.2 (1966) 786.
11. J. AVESTON, G. A. COOPER and A. KELLY, in Single and Multiple Fracture, The Properties of Fibre Composites Conference Proceedings (IPC Science and Technology Press, Guildford, UK, 1971) p. 15.
12. D. B. MARSHALL, B. N. COX and A. G. EVANS, *Acta. Metall.* **33** (1985) 2013.
13. H. L. COX, *Brit. J. Appl. Phys.* **3** (1952) 72.
14. M. SUTCU, *J. Mater. Sci.* **23** (1988) 928.
15. R. M. JONES, "Mechanics of composite materials" (Hemisphere Publishing Corp., New York, 1975) p. 54.

Received 30 July 1992
and accepted 23 February 1993